5-2019

INVESTIGATING THE ROLE OF THE P63 ISOFORM ΔNP63 IN LUNG STEM CELL POPULATIONS AND LUNG CANCER

Sarah J. Wu

INVESTIGATING THE ROLE OF THE P63 ISOFORM ΔNP63 IN

LUNG STEM CELL POPULATIONS AND LUNG CANCER

BY

SARAH JIAXI WU

APPROVED:

Elsa R. Flores, Ph.D.
Advisory Professor

Min Gyu Lee, Ph.D.
Advisory Professor

Russell Broaddus, M.D., Ph.D.

Jichao Chen, Ph.D.

Jonathan Kurie, M.D.

APPROVED:

Dean, The University of Texas
Graduate School of Biomedical Sciences at Houston

INVESTIGATING THE ROLE OF THE P63 ISOFORM ΔNP63 IN LUNG STEM CELL POPULATIONS AND LUNG CANCER

A

DISSERTATION

Presented to the Faculty of

The University of Texas

Health Science Center at Houston

and

The University of Texas

M. D. Anderson Cancer Center

Graduate School of Biomedical Sciences

In Partial Fulfillment

Of the Requirements

For the Degree of

DOCTOR OF PHILOSOPHY

By

Sarah Jiaxi Wu

Houston, Texas

May 2019

Dedication

I dedicate this to my grandfather, Qian Wu, whose stories of perseverance and political persecution showed me what it means to have true grit and whose valiant battle with cancer has been an inspiration and motivator in cancer research.

Acknowledgements

I would like to acknowledge Drs. Elsa Flores and Min Gyu Lee for serving as my PhD mentors. Thanks to Elsa for welcoming me into her lab and having the faith in me to pursue a new project in lung biology. I really appreciate her mentorship and support. Thanks to Min Gyu for warmly welcoming me into his lab and teaching me so much about epigenetics.

Thanks to members of my advisory committee – Drs. Jon Kurie, Jichao Chen, and Russell Broaddus as well as past members – Drs. Ken Tsai and Xiaoping Su. I really appreciated all of your support and feedback on my project.

Thanks to lab members from Flores lab (Marlese, Marco, Xiaohua, Payal, Andrew, Ngoc, Ramon, Brooke, Xiaobo) and Lee lab (Shilpa, Hunain, Tsai-Yu) for all your support. I have always appreciated our great scientific discussions as well as other outings outside of the lab.

Thanks to the G&D graduate program and especially Elisabeth Lindheim. The MD/PhD program has also been supportive. Thanks to my friends in grad school who have made it fun to celebrate as well as commiserate.

Thanks to my family for their support, especially my mother who has tirelessly supported me by coming on weekends to babysit.

Thanks to my daughter Elise for being a bright spot in my day and a blessing in my life. And of course, thanks to my husband Aaron for his unwavering support during every stage of my degree program and life's challenges.

Investigating the role of the p63 isoform ΔNp63 in

lung stem cell populations and lung cancer

Sarah Jiaxi Wu

Supervisory Professor: Elsa R. Flores, Ph.D. and Min Gyu Lee, Ph.D.

Abstract

Cell of origin studies have determined separate populations of lung progenitor cells that give rise to lung adenocarcinoma and squamous cell carcinoma. ΔNp63 is known to regulate lung development but its role in lung cancer progression remains unclear. We utilized a ΔNp63-specific conditional knockout mouse model to determine ΔNp63's role in lung progenitor cells and lung cancer. In vivo and in vitro experiments revealed a role for ΔNp63 in maintaining lung progenitor cells. ChIP-seq results indicate that deletion of ΔNp63 results in robust loss of enhancer histone marks at cell identity genes for lung progenitor populations of basal cells and AT2 cells. Analysis of ΔNp63-regulated pathways uncovered that ΔNp63 regulates cell-type-specific genes as well as common genes for basal cells and AT2 cells. Our experiments using a deactivated cas9 system showed that co-targeting of ΔNp63 and the enhancer activator p300 to p63 binding motifs significantly enhanced the transcription of ΔNp63-regulated genes, indicating that ΔNp63 directly regulates enhancer region activity. These novel findings suggest that ΔNp63 acts as a master regulator of transcriptional and epigenetic networks in lung progenitor cells whose oncogenic characteristics are essential to the initiation and progression of lung cancer.

Table of Contents

List of Figures

Chapter 1

Chapter 3

Chapter 5

Chapter 6

1. Chapter 1: Introduction

Chapter 1: Introduction

1.1 Lung Cancer Subtypes, Diagnosis and Treatment

Lung cancer is the number one cause of cancer mortality worldwide, contributing to more deaths than breast, colon, and prostate cancer combined (Siegel et al., 2019)(Siegel et al., 2019)(Siegel et al., 2019). Lung cancer can be divided into two major subtypes: small cell lung cancer and non-small cell lung cancer. Non-small-cell lung cancer (NSCLC) comprises 85% of all lung cancers with adenocarcinoma and squamous cell carcinoma (SCC) as the first and second most common subtypes, respectively. Currently, the mean survival of patients with metastatic NSCLC is around 1 year, with a 3.5% 5-year survival rate (Cataldo et al., 2011).

The high degree of lung cancer mortality can be attributed to a lack of effective diagnostic tools and targeted therapeutics (Herbst et al., 2008). A 2011 SEER cancer statistics review examining at lung cancer diagnosis and survival by stage found that while 5-year survival was at 52% for localized lesions, these comprised only 15% of all diagnoses (Howlader N, 2011). The vast majority of patients were diagnosed when they already had distal metastases (56%) with a 4% 5-year survival. Early diagnosis of lung cancer has been an area of focus, but current options are limited. Current diagnostic modalities for lung cancer include imaging such as computerized tomography (CT) or positron emission tomography (PET) scans (Wang et al., 2018). However, these methods have not been shown to be able to accurately detect small lesions and there is a high false positive rate. This may contribute to the high mortality rate of lung cancer, as there is no reliable method to detect early lesions, whereas breast, colon, and prostate cancer have established protocols for early detection. Development of new diagnostic

mechanisms to determine pre-malignant lesions could be essential to address the high mortality rate of lung cancer.

Because of the poor response to first-line cisplatin-based chemotherapy, therapies against molecular targets have been an area of intense focus. Current guidelines presented at ASCO 2018 suggest tyrosine kinase inhibitors as treatment for tumors with mutations in EGFR, ALK, ROS; cancers lacking mutations are treated with PD-1 inhibitor pembrolizumab in combination with traditional chemotherapeutic agents (Bironzo and Di Maio). The poor prognosis and lack of effective treatment of lung cancer identifies a need to better understand its molecular basis and development in order to develop new targeted therapies.

1.2 Stem Cells as Cells of Origin of Cancer

Adult stem cell populations play an important role in dividing into differentiated cell types as well as self-renewal to maintain the stem cell pool. Due to similarities in signaling pathways and self-renewal abilities between transformed cells and stem cells, it is hypothesized that cancer may originate from transformed stem cells (Reya et al., 2001, Visvader, 2011). As differentiated cells rarely self-renew or divide, any mutations incurred in these cells are not maintained in the population. However, the adult stem cells are able to self-renew and create a population of cells maintain any oncogenic mutation, especially those with mutations that promote growth-signaling pathways. Subsequent mutations in this cell population leads to expansion of the population and eventual progression into a tumor. As the pathogenesis of lung cancer is often due to exposure to carcinogenic agents like smoking over a prolonged period of time, the transformed stem cell hypothesis is particularly relevant.

1.3 Lung Stem Cell Populations and Role as Cells of Origin for Cancer

There are numerous stem cell populations of the lung, which are involved in regeneration of distinct regions (Eramo et al.). The lung can be separated into two main compartments with differing cellular makeup. The proximal lung is comprised of the trachea and bronchioles, which are responsible for transporting and conditioning air that's breathed in. The main stem cell population of the proximal lung is the basal cell. The basal stem cells of the trachea differentiate into ciliated and goblet cells (Rock et al.) and are thought to be the cell of origin for lung SCC as both populations express similar histological markers p63 and keratin 5 (Krt5) (Hanna and Onaitis, 2013). Jeong et al. recently published that overexpression of KEAP1 and deletion of p53 in basal cells can result in development of lung SCC in mice (Jeong et al.).

The distal lung is comprised of the alveolar structures that promote gas exchange. The two main epithelial cell populations are type I alveolar cells (AT1) and type II alveolar cells (AT2) (Sutherland and Berns). Kim et al. identified a population of bronchioalveolar stem cells (BASCs), which exhibited stem-like properties and were hypothesized to be the cell of origin for adenocarcinoma (Kim et al., 2005). Xu et al. demonstrated that while BASCs could progress to hyperplasia, only the type II alveolar cells, a multipotent cell responsible for maintaining cells in the alveoli, could form adenocarcinomas (Xu et al., 2012).

1.4 p53 Family of Transcription Factors

p53 is known as the guardian of the genome and is responsible for maintaining genomic integrity of the cell. Sequencing initiatives like the Cancer Genome Atlas (TCGA) have found p53 to be the most commonly mutated or deleted gene in the majority of cancers, demonstrating its importance in the pathogenesis of cancer. P53 is

a transcription factor that is able to form tetrameric complexes and promote transcription of key genes involved in DNA damage and apoptosis response. Efforts have been made to target p53 pharmacologically with limited success. Because of the frequent deletion and mutation of p53, an alternative strategy is to look to the other members of the family to target p53 signaling pathways.

Other family members, p63 and p73, have been found to have similar structure to p53, but also with distinct functions. P63 specifically has been found to have two major isoforms, which arise from distinct promoters: TAp63 and ΔNp63. TAp63 has tumor suppressive functions (Su et al.) while ΔNp63 generally has oncogenic properties (Figure 1). The mechanisms of ΔNp63 tumorigenesis are diverse, including dominant negative antagonism of p53, regulation of miRNA biogenesis, and direct transcriptional targets (Chakravarti et al., 2014, Tran et al., 2013). Because of the difficult nature of distinguishing the isoforms, p63 isoforms have been lumped together and their individual functions have been difficult to discern. By use of specific isoform knockout mouse models, the distinct functions of TAp63 and ΔNp63 can be elucidated.

Our laboratory has developed p63 isoform specific conditional knockout mouse models to study the individual functions of these isoforms, focusing on their roles in stem cell maintenance and in tumorigenesis. Our lab has shown that in the epidermis, TAp63 and ΔNp63 regulate distinct stem cell populations; TAp63 maintains stem cells in the dermal papilla while ΔNp63 maintains epidermal basal cells (Su et al., 2009). We have demonstrated that ΔNp63 is critical for terminal differentiation of the epidermis (Chakravarti et al., 2014) and acts as an oncogene by inhibiting p53, TAp63, and TAp73 function (Venkatanarayan et al., 2015). Importantly, we have also identified novel ways of therapeutically targeting cancers through manipulation of ΔNp63 (Napoli et al., 2016).

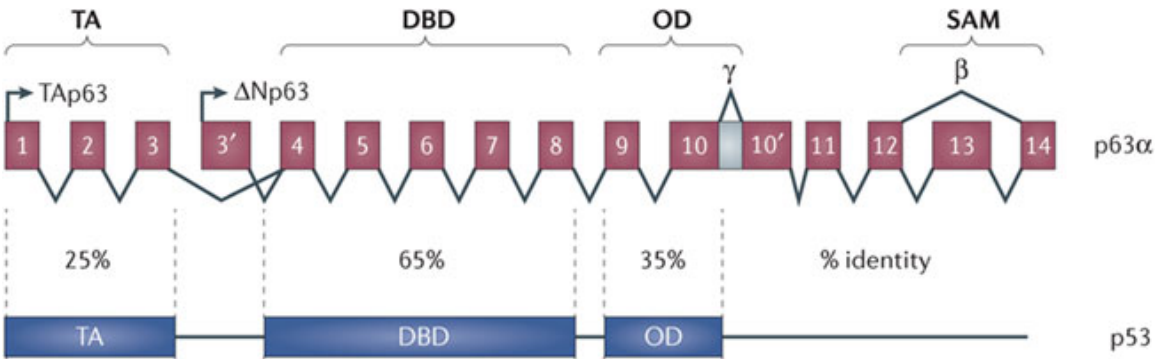

Figure 1: Structure of p63 gene in comparison to p53.

The structure of the p63 gene has similarity to p53(Su et al., 2013). P63 has two promoters that result in transcription of unique isoforms. The promoter at exon one leads to transcription of the TAp63 isoform, which contains a transactivation domain (TA) as well as the DNA-binding domain (DBD) and oligomerization domain (OD). The ΔNp63 isoform is transcribed from an alternative promoter at the 3' exon and does not contain the transactivation domain. In addition to variability at the N-terminal, there exist splice variants at the C-terminal, some of which contain a sterile alpha motif (SAM) domain.

Figure used with permission from Su X, Chakravarti D, Flores ER. p63 steps into the limelight: crucial roles in the suppression of tumorigenesis and metastasis. Nat Rev Cancer. 2013 Feb;13(2):136-43. License number: 4384531506832.

1.5 Role of p63 in Lung Stem Cells and Lung Cancer

The transcription factor, p63, a member of the p53 family, is expressed in the basal stem cells of the lung (Wansleeben et al., 2013, Daniely et al., 2004) and is a master regulator of stem cell maintenance and differentiation of epithelial tissues (Su et al., 2013). The characterization of the role of p63 in the lung epithelium is complex, as there are two isoforms with distinct roles, TAp63 and ΔNp63. ΔNp63 was identified as significantly altered in 44% of primary lung squamous cell carcinomas by the Cancer Genome Atlas (TCGA) (Cancer Genome Atlas Research, 2012). Compared to p53, which is commonly mutated, p63 is often amplified in both lung squamous cell carcinoma and lung adenocarcinoma (Figure 2). Analysis of TCGA RNA-seq data using SpliceSeq (Ryan et al., 2012) shows ΔNp63 is the main p63 isoform expressed in lung squamous cell carcinoma and the classical molecular subtype has the highest ΔNp63 expression (Figure 3). ΔNp63 has been identified as an oncogene in squamous cell carcinoma of the skin, which shares molecular characteristics and p63 expression patterns with lung SCC (Yan et al., 2011). Our lab's analysis comparing the ΔNp63 gene signature generated from keratinocytes and lung SCC from TCGA also identify ΔNp63 as a putative oncogene (Abbas et al., 2018). p63, specifically ΔNp63 or p40, has been utilized as a diagnostic marker for lung squamous cell carcinoma (Daniely et al., 2004). P63 staining is visible in the nuclei of basal cells of the tracheal epithelium. Squamous metaplasia and squamous cell carcinoma tissue also stains positive for p63 (Daniely et al., 2004). While ΔNp63 staining is considered specific and diagnostic for lung squamous cell carcinoma, a small percentage of lung adenocarcinomas also stain positive for ΔNp63. A study of 150 adenocarcinoma samples demonstrated positive staining in 27 tumors (18%) (Nonaka, 2012). The relative lack of mechanistic understanding of p63 isoforms in the lung necessitates further study.

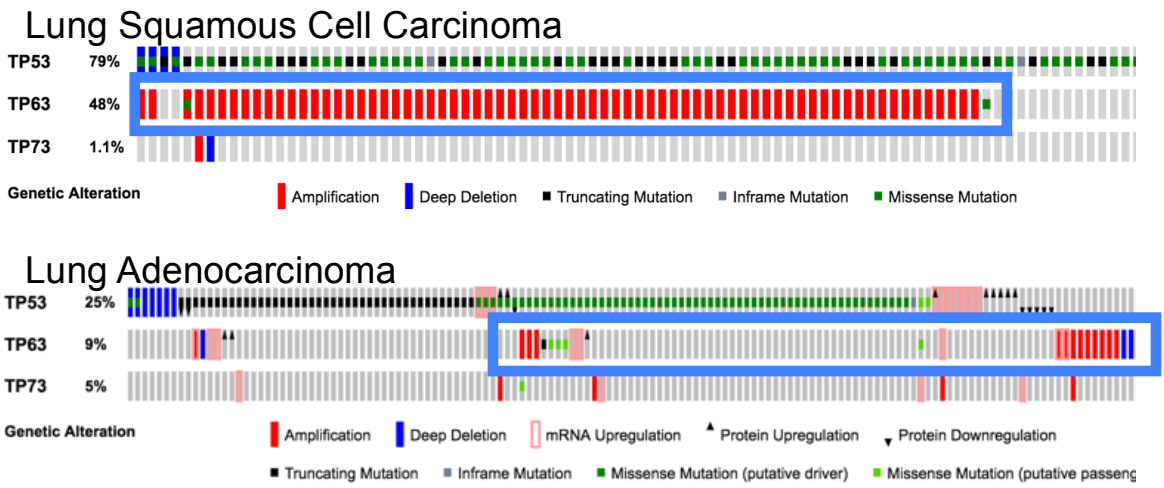

Figure 2: p53 family alterations in TCGA lung squamous cell carcinoma and lung adenocarcinoma.

A comparison of p53 family members TP53, TP63, and TP73 in lung squamous cell carcinoma and lung adenocarcinoma. While TP53 is more often mutated in lung cancer, TP63 is amplified in both lung squamous cell carcinoma and lung adenocarcinoma. Cbioportal data, TCGA (LUSC and LUAD, all samples).

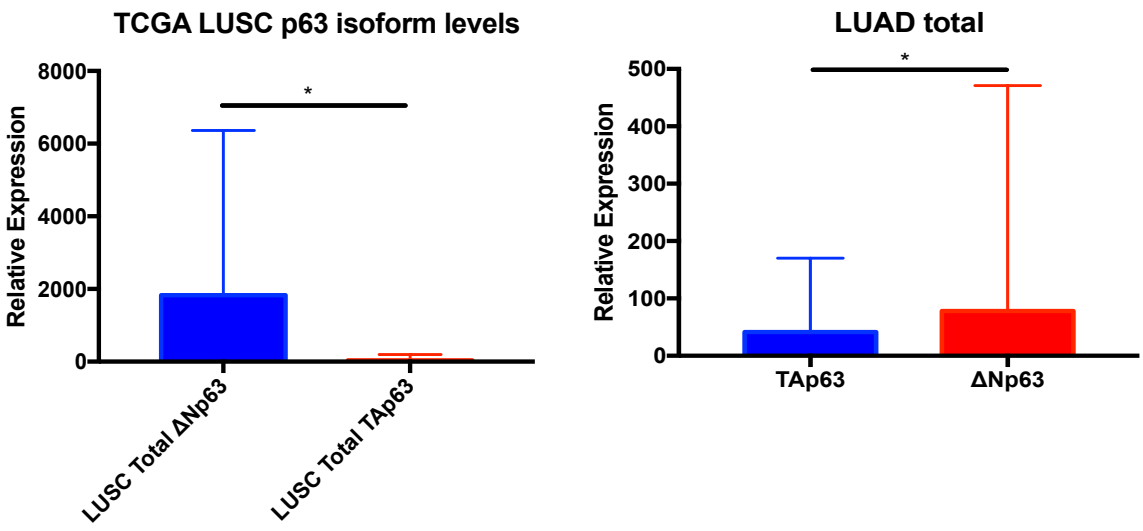

Figure 3: p63 isoform levels in TCGA lung squamous cell carcinoma (LUSC) and lung adenocarcinoma (LUAD).

Analysis of RNA sequencing data from the TCGA lung squamous cell carcinoma (LUSC) and lung adenocarcinoma (LUAD) datasets. While both LUSC and LUAD have statistically significantly higher levels of ΔNp63 mRNA compared to TAp63, levels of ΔNp63 mRNA are significantly higher in LUSC (average relative expression of 2000 vs 100).

1.6 Epigenetics in Cell Identity and Development of Cancer

While cancer biology has long focused on gene mutations as drivers of tumorigenesis, increasingly focus has turned to epigenetic regulation of gene expression as a key contributor to the etiology of cancer. Recent work has identified epigenetic mechanisms of gene regulation as key modulators of cancer progression. These processes can dynamically change gene regulation without changes to the DNA, allowing for fast adaptation. Enhancers have been identified as key spatiotemporal regulators of gene expression. Enhancer elements are distant from the promoter and have been shown to have the ability to loop around to interact with the promoter and recruit transcription factors, mediator proteins, and RNA polymerases. Enhancers are commonly marked by two histone modifications: acetylated H3K27 (H3k27ac) and monomethyl H3K4 (H3K4me1). Enhancers which cluster together in large regions of the genome over 10 kilobases are deemed super-enhancers and have been associated with genes that designate cell identity (Whyte et al., 2013). Interest has grown in understanding the regulation of super-enhancers as super-enhancer-associated genes are the most highly expressed in the cell and are thought to play a key role in the biology of the cancer (Sur and Taipale, 2016). Recent development of pharmacologic mechanisms to target super-enhancer biology has also increased interest in understanding more about how cancer cells epigenetically regulate gene expression.

2. Chapter 2: Materials and Methods

Chapter 2: Materials and Methods

2.1 Mouse Genotypes

The following mouse strains were generated:

$\Delta Np63^{fl/fl}$; $Rosa^{M/M}$

$TAp63^{fl/fl}$; $Rosa^{M/M}$

$LSLKras^{G12D/+}$; $Rosa^{M/M}$

$\Delta Np63^{fl/fl}$; $LSLKras^{G12D/+}$; $Rosa^{M/M}$

$\Delta Np63^{fl/fl}$ and $TAp63^{fl/fl}$ mice were generated in the Flores lab (Su et al., 2010, Chakravarti et al., 2014). $LSLKras^{G12D/+}$ and $Rosa^{M/M}$ mice were purchased from Jackson labs and National Institutes of Health.

2.2 Mouse Husbandry

Mice were aged until 6-8 weeks old before being utilized in experiments. Both male and female mice were used at equal ratios. Littermates were randomly assigned to experimental groups. Animals were maintained according to established protocols approved by the Institutional Animal Care and Use Committee of MD Anderson Cancer Center and Moffitt Cancer Center.

2.3 Mouse Tissue Processing

Lung tissue was isolated from a euthanized mouse and preserved in 10% formaldehyde for 24 hours, followed by preservation in 70% ethanol for 24 hours. Lung and trachea tissue were then processed and embedded into paraffin by the MD Anderson Research Histology Core Lab.

2.4 Immunohistochemistry

Unstained slides were dewaxed and rehydrated by washing in sequential rinses of xylene, 100% ethanol, 90% ethanol, 70% ethanol, and PBS. Following this step is three washes of PBS/0.2% Triton-X-100 to enable permeabilization of tissues. Blocking was performed with PBS/10% normal donkey serum.

2.5 Microscopy and Image Processing

Bright field and immunofluorescence images were taken on an Olympus IX83 microscope. Images were processed in Adobe Photoshop.

2.6 Image Quantification

Immunohistochemical and immunofluorescence images were quantified using ImageJ cell counting software.

2.7 Intratracheal Infection of Mice

6-8 week old mice were anesthetized with a ketamine/xylazine (ketamine 100 mg/kg IP, xylazine 10 mg/kg IP), intubated using a fiber optic illuminated catheter (DuPage et al., 2009), and given $2.5x10^7$ PFU viral dosage suspended in 100 microliters of minimal essential media (MEM). CMV-cre and CMV-empty adenovirus was obtained from the BCM viral core**.**

2.8 Scoring of Tracheal Sections

3 H&E sections of trachea cut 50 μms apart per mouse were analyzed using the Olympus Cellsense software. Tracheal epithelial height was measured from the basement membrane to the apex of the membrane. Epithelial separation was defined as length of epithelium where the basement membrane was separated.

2.9 Lung Tumor Grading

H&E sections of mouse lungs were examined and lung lesions were graded into atypical adenomatous hyperplasia (AAH), grade 1, and grade 2+ (Jackson et al., 2001). For each mouse, 3 H&E sections of 5 lung lobes taken 100 μms apart were analyzed.

2.10 Polidocanol Administration

50 μl of 2% polidocanol was administered to the mouse trachea by a catheter inserted into the trachea (Paul et al., 2014, DuPage et al., 2009).

2.11 Cell Culture of Tumor Cell Lines

The following human cell lines were utilized: H520, H2170, H358. Cells were cultured at 37C in 5% CO2 conditions. RPMI media supplemented with 1% L-glutamine, 1% penicillin/streptomycin, and 10% FBS. Cell lines were authenticated by STR profiling (MD Anderson Cell Line Authentication Service).

2.12 Mouse Tumor Xenografts

$5x10^6$ human lung cancer cells were mixed in 1:1 ratio with growth factor reduced matrigel in a total volume of 200 microliters to inject per flank in nude mice. Male nude mice were utilized for xenograft studies. Mice were injected with control cell line in the left flank and experimental cell line in the right flank. Tumors were measured weekly with calipers until one side's final volume reached around 2 cm^3. Mice were euthanized and the tumors were excised, measured, fixed in 10% formaldehyde, and submitted for histological processing.

2.13 Tumor Cell Line Soft Agar Colony Assay

Human lung cancer cell lines were plated in 100 μl of 1:1 ratio of RPMI: growth factor reduced matrigel at 100 cells per well in a 96 well plate, with 100 μl of RPMI media plated on top of the matrigel layer. The top 100 μl of RPMI was changed every 2 days.

To analyze colony numbers, the matrigel was dissolved with cell recovery solution (Corning) at 4C for 1 hour and the plate was scanned using the Celigo colony analysis software.

2.14 Isolation of Mouse Basal Stem Cells

The tracheas from $\Delta Np63^{fl/fl}$; $Rosa^{M/M}$ mice were isolated and digested with papain at 37 degrees Celsius (Rock et al., 2009). Basal cells were cultured on mitomycin treated J2-3T3 feeders for 7 days in MTEC media with rock inhibitor.

2.15 Adenovirus Infection of Cells *In Vitro*

Cells were infected at a multiplicity of infection (MOI) of 100. Adenovirus (adeno-empty and adeno-cre) was added to cells in a total volume of 2 ml and incubated at 37C for 1 hour, agitating every 15 minutes. Cells were then washed with PBS.

2.16 Basal Stem Cell Proliferation Assay

Basal cells were plated on a bed of mitomycin treated J2-3T3 feeders. EdU was added to the media for 24 hours. Cells were fixed with paraformaldehyde and developed using the Click-it EdU Alexa Fluor 488 imaging kit (Invitrogen). Data was analyzed on the Nexcelom Celigo.

2.17 Basal Stem Cell Sphere Formation Assay

Basal cells in single cell suspension were seeded into 100 µl of 1:1 growth factor reduced matrigel:MTEC media in a 96 well plate. 100 µl of MTEC plus media was seeded on top of the matrigel. Media was changed every 2 days. Cells were grown for 1 week. Matrigel was dissolved with cell recovery solution (Corning) and the plate was placed at 4C for 2 hours to allow the spheres to sink to the bottom of the plate. The plate was then scanned and analyzed on the Nexcelom Celigo.

2.18 Basal Stem Cell Differentiation Assay

Basal cells were seeded into 1:1 GFR matrigel: MTEC plus media into a 24 well plate insert. MTEC plus media in the well was changed every 2 days and rock inhibitor was omitted after day 4 to allow for differentiation. After 20 days of growth, the media was removed and replaced with 4% paraformaldehyde for 24 hours of fixation. The fixed matrigel sample was removed and embedded in Histogel, followed by histological processing.

2.19 Basal Stem Cell Apoptosis Assay

Basal cells were plated on top of mitomycin treated J2-3T3 feeders. Using the Annexin V/Dead Cell Apoptosis Kit (Thermo Fisher), cells were incubated with reagent and subsequently fixed. Analysis was conducted using the Nexcelom Celigo for imaging.

2.20 Distal Lung Stem Cell Isolation Assay

BASCs and AT2 cells were isolated from $\Delta Np63^{fl/fl}$; $Rosa^{M/M}$ mice (Kim et al., 2005, Driscoll et al., 2012). After digestion with collagenase and dispase, cells were stained with fluorescent antibodies: CD31-APC BD #551262, CD45-APC BD #559864, EpCAM-PE-Cy7 BioLegend #118216, and SCA-1-APC-Cy7 BD #560654. Cells were sorted in a MoFlo Astrios cell sorter. AT2 cells are contained in the $CD31^{neg}$, $CD45^{neg}$, $EpCAM^{pos}$ and $Sca\text{-}1^{neg}$ population and BASCs, in the $CD31^{neg}$, $CD45^{neg}$, $EpCAM^{pos}$ and $Sca\text{-}1^{pos}$ population.

2.21 Distal Lung Stem Cell Colony Formation Assay

BASC and AT2 cells were plated in a gelatin coated 96-well plate mixed with primary mouse lung endothelial cells in a ratio of 1000 stem cells to $2x10^6$ endothelial cells per

plate. Media was changed every 2 days. The plate was analyzed on the Nexcelom Celigo after 1 week of culture (Kim et al., 2005) using the colony counting algorithm.

2.22 RNA Isolation

RNA was extracted using trizol extraction and the Ambion Pure Link RNA mini kit. 10 µl of glycogen was added in the wash step to promote isolation of small RNAs.

2.23 TCGA Data Analysis

The primary and processed data tumor and normal samples were downloaded from The Cancer Genome Atlas at (https://tcga-data.nci.nih.gov/tcga/tcgaDownload.jsp) between July 2014 and February 2015. First, RNA-sequencing data for each tumor were quantile normalized using R. All differential gene expression and statistical analyses were done using the R statistical system.

2.24 Generation of mouse or human signatures

Approximately 5 µg of polyA+ RNA was used to construct RNA-Seq libraries using the standard Illumina protocol. Mouse and human mRNA sequencing yielded 20-40 million read pairs for each sample. The mouse mRNA-Seq reads were mapped using TopHat v2.0.12 onto the mouse genome mm10 (GRCm38) assembly. Then, mapped reads were assembled using cufflinks v2.2.1 in order to calculate the fragments per kilobase of transcript per million mapped reads (FPKM). A combined profile of all samples was computed. Principal component analysis was executed using the implementation within the R statistical analysis system. Hierarchical clustering of samples was executed by first computing the symmetrical sample distance matrix using the Pearson correlation between mRNA profiles as a metric, supervised sample analysis was performed using the t-test statistics, and heat maps were generated using the heatmap.2 package in R.

2.25 RNA-seq

For small RNA library construction, RNA samples were prepared using the DGE-Small RNA Sample Prep Kit (Illumina, San Diego, CA) as described previously (16, 17). A total of two Solexa-ready small RNA templates were analyzed on an Illumina GA-IIx Genome Analyzer at University of Houston. Cluster generation was performed and clusters were sequenced. Initial sequence process and analysis was followed as described previously (16, 17). Small RNA-Seq sequencing data was uploaded and processed using the Genboree Small RNA Toolset (http://genboree.org). The Illumina adapter was trimmed, and reads with length between 11 and 30, a copy number of at least 4, and finishing in monomers with length less than 10, were selected for further processing, similar to the processing described previously (16, 17). The reads were mapped to the mouse genome and build UCSC mm9 (NCBI 37) using Pash 3.0(18). Reads mapping up to 100 locations were selected for further analysis. The miRNA definitions from miRBase (19-22) were used to construct a known miRNA profile for each sample; the abundance of the known miRNAs was normalized as a fraction of the usable reads. For each species, a combined profile of all samples was computed; miRNA abundance was mean-centered and z- score transformed for each miRNA individually. Principal component analysis was performed using the implementation within the R statistical analysis system. Hierarchical clustering of samples was performed by first computing the symmetrical sample distance matrix using the Pearson correlation between microRNA profiles as a metric. Supervised sample analysis was performed using the t-test statistics, and heat maps were generated using the heatmap.2 package in R.

2.26 Low Cell Number ChIP-seq

Cells were pelleted and snap-frozen using liquid nitrogen. Low cell number ChIP-seq was performed at Active Motif, for wild type and ΔNp63 knockout samples, for H3K27ac,

Pol2, and ΔNp63 ChIP-seq. Sequencing was analyzed by HOMER to identify peaks that contained the p63 transcription factor binding motif.

2.27 qPCR Analysis

cDNA was synthesized using Bio-Rad cDNA synthesis kit. qPCR was performed by Bio-Rad master mix.

2.28 dCas9 Experiments

Experiments were performed in 293T cells (Wang et al., 2017, Hilton et al., 2015). ΔNp63 was cloned into the dCas9 vector. 4 sgRNAs per genomic site were designed using the Broad sgRNA design tool. sgRNA sequences were cloned into PLX-sgRNA vector. Plasmids for dCas9, dCas9-p300 and dCas9-ΔNp63 were utilized in a 3:1 ratio to sgRNA vectors. All plasmids were transfected using Lipofectamine 2000. Cells were incubated for 48 hours before collection of the RNA. Gene expression was measured by qPCR analysis.

3. Chapter 3: Functions of p63 isoforms in basal cell of the trachea.

Chapter 3: Functions of p63 isoforms in basal cell of the trachea.

3.1 *In vivo* ΔNp63 deletion in tracheal epithelium results in expansion and depletion of apoptotic Krt5+ basal cells.

To determine the role of ΔNp63 in the normal mouse lung, we crossed the $\Delta Np63^{fl/fl}$ mice to the Rosa reporter mouse to enable identification of cells that have undergone recombination, signified by a switch from tdTomato (red) to GFP (green) expression. To specifically target lung epithelium, we performed an intratracheal infection of $\Delta Np63^{fl/fl}$; $Rosa^{M/M}$ mice with adenoviral cre-recombinase, with adenoviral empty vector serving as the control. Histological analysis of the trachea and lung tissues of the mice was performed at 1 month and 3 month post-induction time points. Immunohistochemical staining for ΔNp63 showed loss of expression in the tracheal epithelium of $\Delta Np63^{\Delta/\Delta}$; $Rosa^{\Delta/\Delta}$ mice but was maintained in control and $TAp63^{\Delta/\Delta}$; $Rosa^{\Delta/\Delta}$ mice (Figure 4). At 1 month post-induction, quantification of H&E stained sections of $\Delta Np63^{\Delta/\Delta}$; $Rosa^{\Delta/\Delta}$ tracheal epithelium showed a significant increase of stratified epithelium (SE) and epithelial separation (ES) per microscopic field compared to the control (Figure 5B). Staining for basal cell marker keratin 5 (Krt5) revealed that the make-up of the stratified epithelium in $\Delta Np63^{\Delta/\Delta}$; $Rosa^{\Delta/\Delta}$ tracheal epithelium was primarily Krt5+ basal cells (Figures 5A) whereas the ad-empty control maintained a single basal layer of Krt5+ cells. $\Delta Np63^{\Delta/\Delta}$; $Rosa^{\Delta/\Delta}$ Krt5+ cells were also significantly more positive for Ki67 staining compared to control. At the 3-month time point, the majority of the $\Delta Np63^{\Delta/\Delta}$; $Rosa^{\Delta/\Delta}$ tracheal epithelium exhibited a hypoplastic epithelial (HE) phenotype (Figure 6B) compared to the pseudostratified columnar appearance of the control epithelium. Krt5 staining of $\Delta Np63^{\Delta/\Delta}$; $Rosa^{\Delta/\Delta}$ tracheal epithelium showed decreased abundance of Krt5+ basal cells (Figure 5A), suggesting a depletion or exhaustion of basal cells after loss of ΔNp63. To determine the mechanism of loss of

basal cells, we stained the epithelium for apoptotic marker, cleaved caspase 3. We observed positive staining in the proliferating cells in the 1-month ΔNp63 knockout mice. ΔNp63 is highly expressed in the basal cell population of the trachea and basal cells, which have been shown to be cells of origin for lung squamous cell carcinoma (Jeong et al., 2017). At an extended time point of 6 months post-induction, ΔNp63Δ/Δ tracheal epithelium was observed to have a similar flattened phenotype with basement membrane separation as the 3-month post-induction time point (Figure 7). This phenotype was not observed in the wild type or TAp63 tracheal epithelium. We conclude that the ΔNp63 is a critical factor for maintenance of the tracheal basal cell and deletion of ΔNp63 results in the loss of self-renewal of the basal cell.

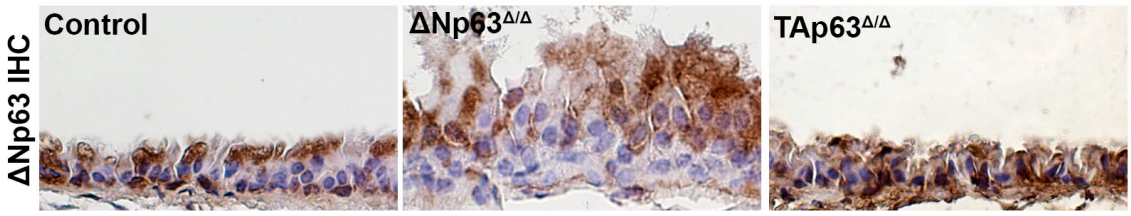

Figure 4. ΔNp63 IHC staining of tracheal epithelium

ΔNp63 immunohistochemical staining of control, $\Delta Np63^{\Delta/\Delta}$ and $TAp63^{\Delta/\Delta}$ tracheal epithelium. $\Delta Np63^{\Delta/\Delta}$ staining was not present in the basal cells of the $\Delta Np63^{\Delta/\Delta}$ epithelium but was still detectable in control and $TAp63^{\Delta/\Delta}$ epithelium.

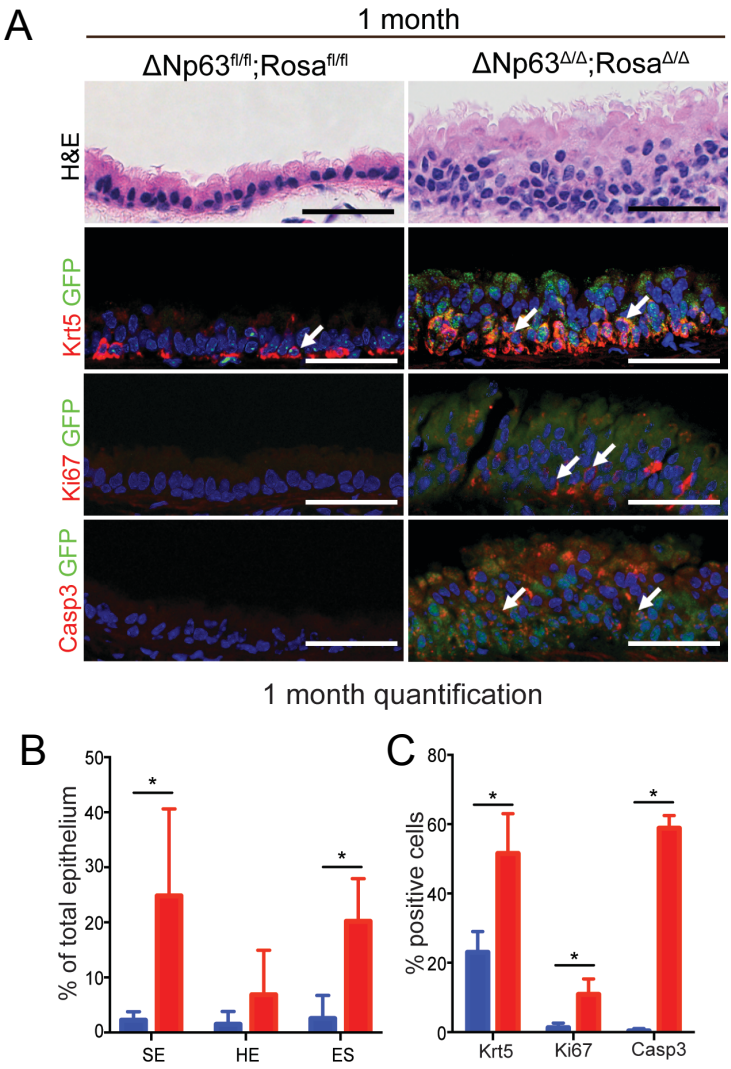

Figure 5: *In vivo* ΔNp63 deletion in tracheal epithelium results in expansion of apoptotic Krt5+ basal cells at the 1 month time point.

A. $\Delta Np63^{fl/fl}$; $Rosa^{M/M}$ and $\Delta Np63^{\Delta/\Delta}$; $Rosa^{\Delta/\Delta}$ tracheal epithelium at 1 month post-induction: H&E, Krt5/GFP, Ki67/GFP, and Casp3/GFP. Scale bar equals 100 μm.

B. Quantification of stratified epithelium (SE), hypoplastic epithelium (HE), and epithelial separation (ES) for $\Delta Np63^{fl/fl}$; $Rosa^{M/M}$ and $\Delta Np63^{\Delta/\Delta}$; $Rosa^{\Delta/\Delta}$ tracheal epithelium at 1 month post-induction.

C. Quantification of immunofluorescence staining of Krt5, Ki67, and Casp3 for $\Delta Np63^{fl/fl}$; $Rosa^{M/M}$ and $\Delta Np63^{\Delta/\Delta}$; $Rosa^{\Delta/\Delta}$ tracheal epithelium at 1 month post-induction.

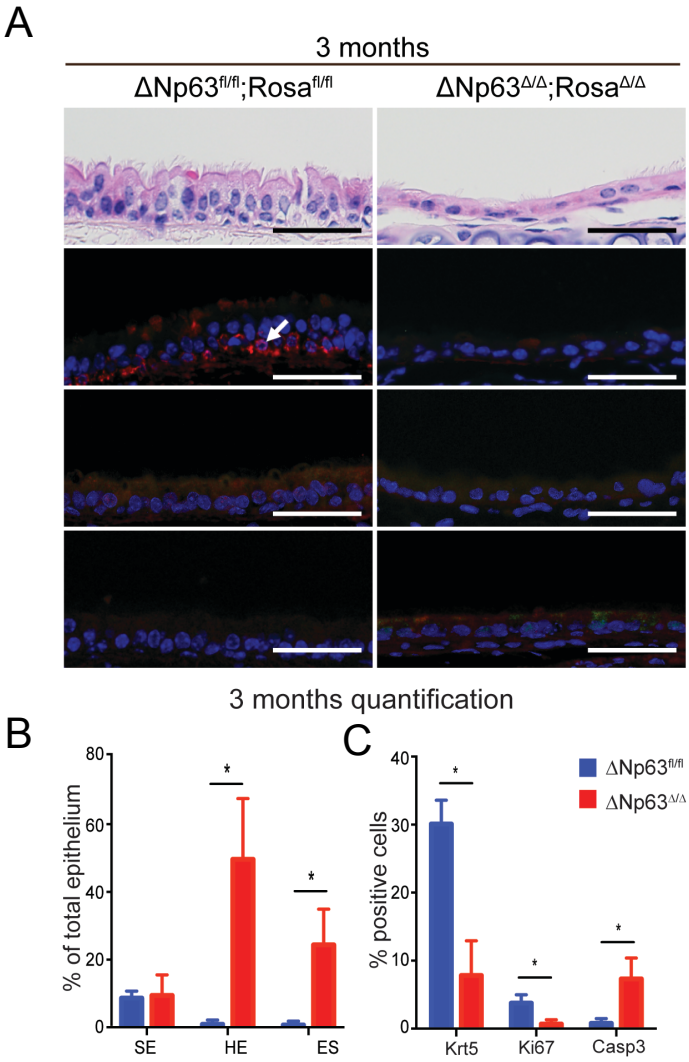

Figure 6. *In vivo* ΔNp63 deletion in tracheal epithelium results in loss of apoptotic basal cells at the 3 month time point.

A. ΔNp63$^{fl/fl}$; Rosa$^{M/M}$ and ΔNp63$^{\Delta/\Delta}$; Rosa$^{\Delta/\Delta}$ tracheal epithelium at 3 months post-induction: H&E, Krt5/GFP, Ki67/GFP, and Casp3/GFP. Scale bar equals 100 μm.

B. Quantification of stratified epithelium (SE), hypoplastic epithelium (HE), and epithelial separation (ES) for ΔNp63$^{fl/fl}$; Rosa$^{M/M}$ and ΔNp63$^{\Delta/\Delta}$; Rosa$^{\Delta/\Delta}$ tracheal epithelium at 3 months post-induction.

C. Quantification of immunofluorescence staining of Krt5, Ki67, and Casp3 for ΔNp63$^{fl/fl}$; Rosa$^{M/M}$ and ΔNp63$^{\Delta/\Delta}$; Rosa$^{\Delta/\Delta}$ tracheal epithelium at 3 months post-induction.

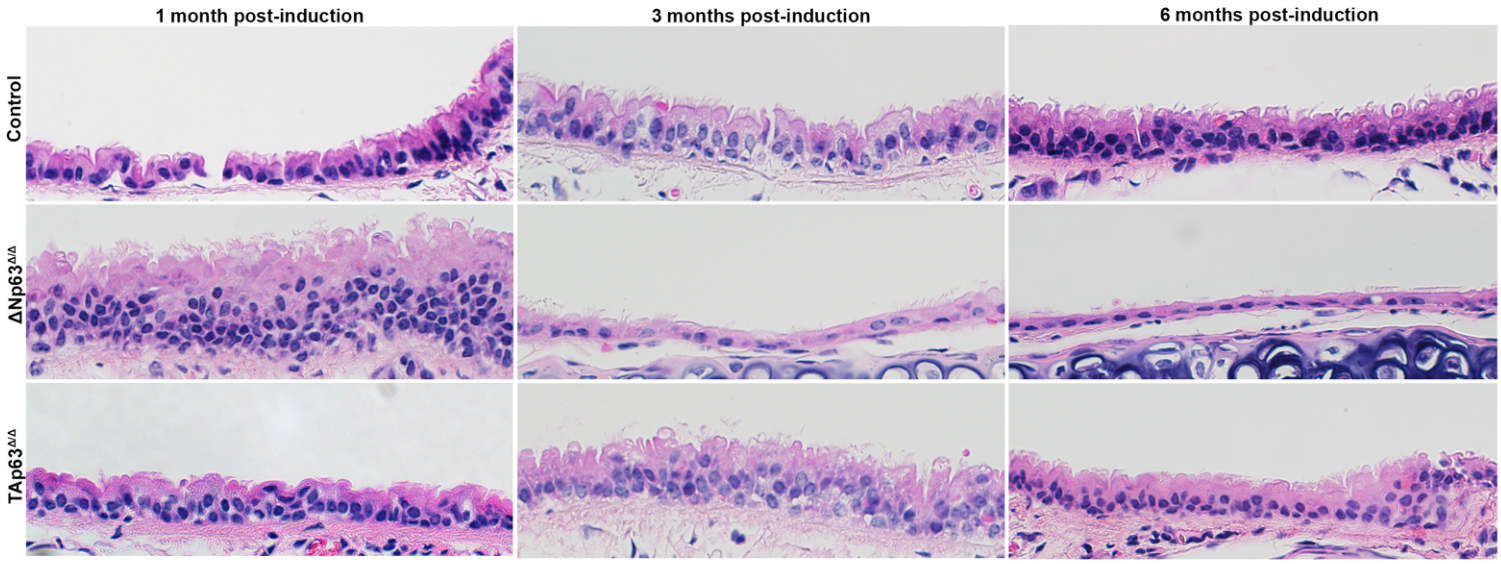

Figure 7. Comparison across time points and genotypes of tracheal epithelium.

H&E images of tracheal epithelium of wild type control, $\Delta Np63^{\Delta/\Delta}$ and $TAp63^{\Delta/\Delta}$ mice across 1 month, 3 month and 6 month time points. Wild type control epithelium retains the pseudostratified columnar architecture of the tracheal epithelium at all time points. The epithelium of the $\Delta Np63^{\Delta/\Delta}$ mouse demonstrates a stratified disorganized epithelium at 1 month, followed by a simplified epithelium at 3 and 6 months. The $TAp63^{\Delta/\Delta}$ epithelium has similar architecture to the wild type control.

3.2 ΔNp63 is required for basal cell differentiation *in vivo.*

As ΔNp63 has been shown to regulate differentiation of stem cells, we asked if ΔNp63-depleted basal cells are able to differentiate into ciliated and goblet cells. To determine the differentiation ability of $\Delta Np63^{\Delta/\Delta}$ basal cells in vivo, we administered a polidocanol challenge to $\Delta Np63^{fl/fl}$; $Rosa^{M/M}$ mice after adeno-cre to remove suprabasal tracheal epithelial cells, leaving a monolayer of basal cells (Figure 8). While the wild type basal cells were able to differentiate into goblet (muc5ac) and ciliated cells (acetylated tubulin) of the tracheal epithelium 1 week after the polidocanol challenge with a pseudostratified columnar structure of the epithelium (Figure 9A), we observed that the $\Delta Np63^{\Delta/\Delta}$ tracheal epithelial forming a stratified epithelium (Figure 10B) of Krt5+ cells (Figure 9B and 9D) that are highly proliferative (Figure 9J) with elevated markers of cell death (Figure 9L). This data suggests that the proliferation of $\Delta Np63^{\Delta/\Delta}$ tracheal epithelium at the 1 month time point is primarily due to basal cell proliferation and not a compensatory dedifferentiation of the ciliated or goblet cells. $\Delta Np63^{\Delta/\Delta}$ mice also exhibited higher mortality after polidocanol treatment compared to $\Delta Np63^{fl/fl}$ mice, with 50% mortality within 4 days of polidocanol treatment, suggesting a decreased ability to maintain a functional tracheal epithelium. We examined the tracheal epithelium at 1 month after polidocanol administration and found that the $\Delta Np63^{\Delta/\Delta}$ mice treated with polidocanol had a thin, hypoplastic epithelium lacking Krt5+ cells (Figures 10B and 10D), similar to the three-month time point of the $\Delta Np63^{\Delta/\Delta}$ mice, suggesting that polidocanol treatment depleted the basal cell population. This data demonstrates the importance of ΔNp63 for maintenance of tracheal epithelial integrity though regulation of basal cell self-renewal and differentiation.

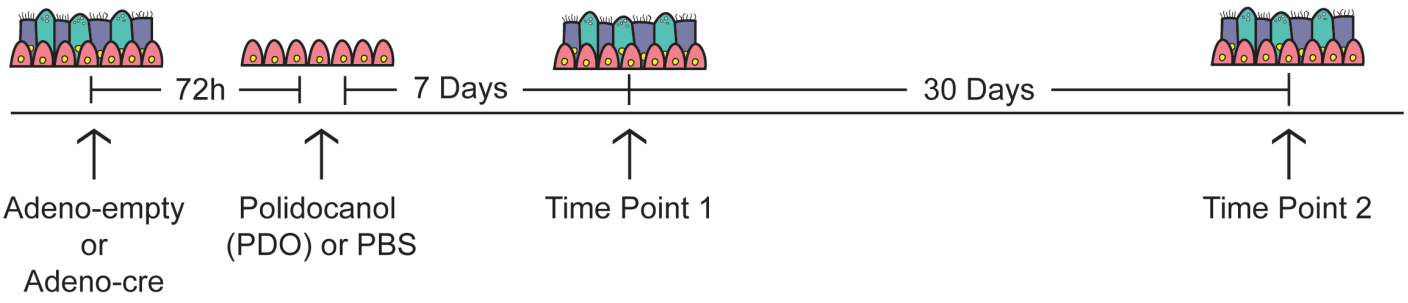

Figure 8. Schematic of polidocanol tracheal injury experiment to determine if ΔNp63 is required for basal cell differentiation *in vivo.*

6-8 week old mice were intratracheally instilled with either adeno-empty or adeno-cre. After 72 hours to allow for recombination, mice were again intratracheally instilled with either polidocanol or PBS. Mice were analyzed at the 7 day time point (time point 1) and after 30 days (time point 2).

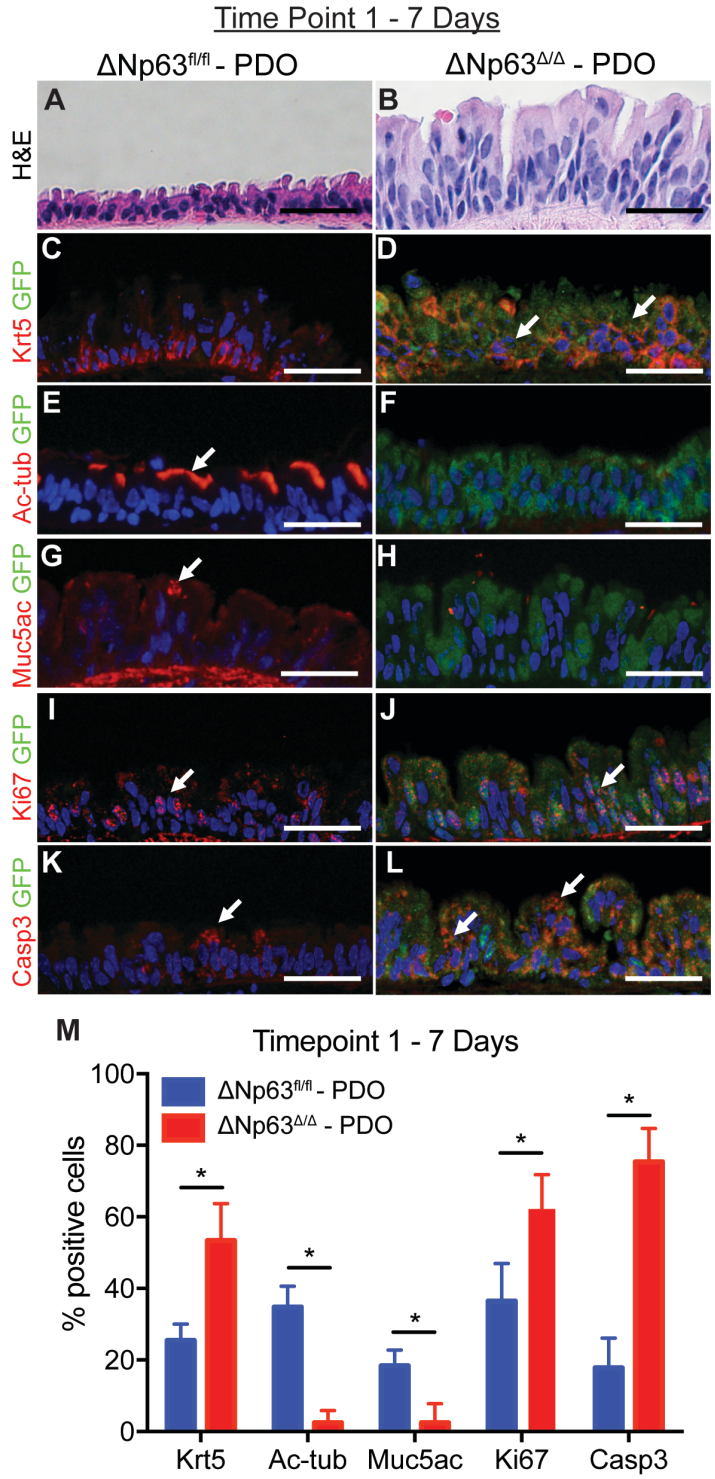

Figure 9. ΔNp63 deletion impairs tracheal epithelial basal cell differentiation.

(A, C, E, G, I, K) ΔNp63$^{fl/fl}$; Rosa$^{M/M}$ tracheal epithelium after polidocanol (PDO) treatment: H&E (A), Krt5/GFP (C), Ac-tub/GFP (E), Muc5ac/GFP (G), Ki67/GFP (I) and Casp3/GFP (K). Scale bar equals 100 μm.

(B, D, F, H, J, L) $\Delta Np63^{\Delta/\Delta}$; $Rosa^{\Delta/\Delta}$ tracheal epithelium after polidocanol (PDO) treatment: H&E (B), Krt5/GFP (D), Ac-tub/GFP (F), Muc5ac/GFP (H), Ki67/GFP (J) and Casp3/GFP (K). Scale bar equals 100 μm.

(M) Quantification of staining for time point 1.

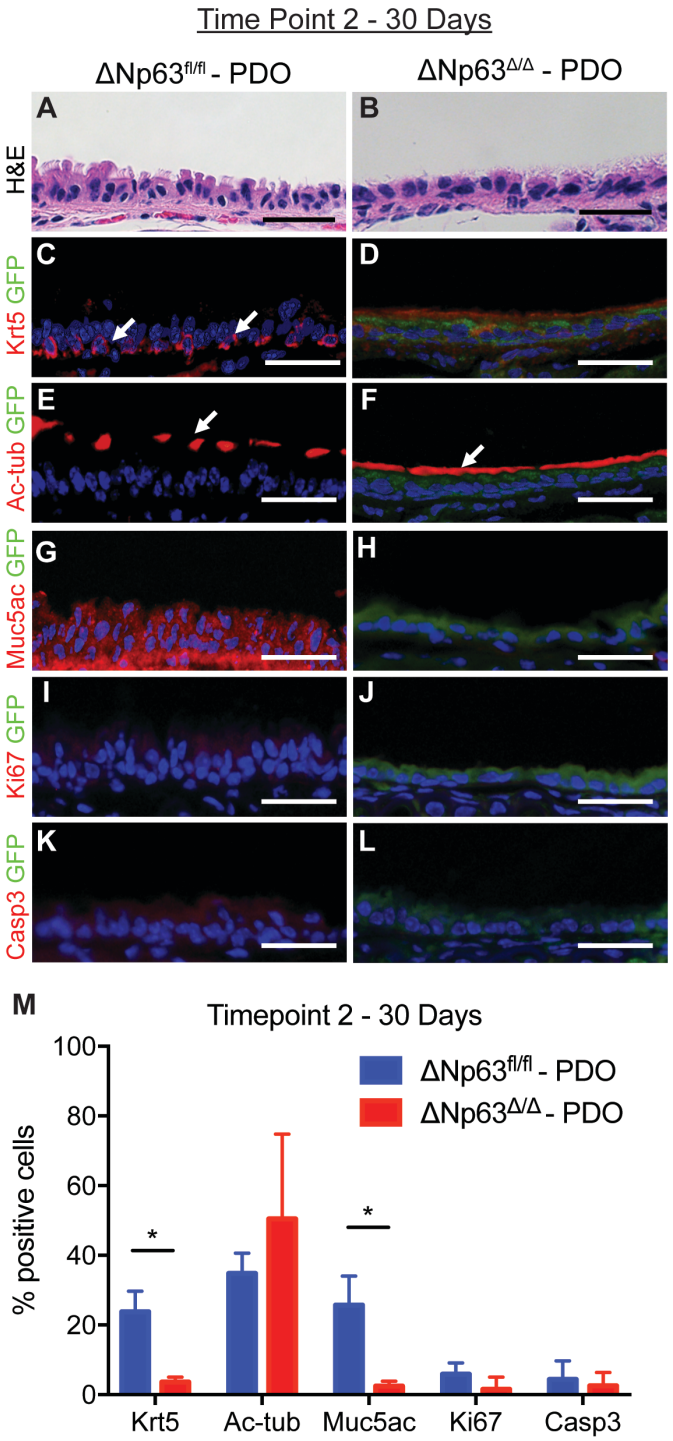

Figure 10. ΔNp63 deletion results in exhaustion of Krt5+ basal cells in polidocanol tracheal injury model.

(A, C, E, G, I, K) ΔNp63$^{fl/fl}$; Rosa$^{M/M}$ tracheal epithelium after polidocanol (PDO) treatment: H&E (A), Krt5/GFP (C), Ac-tub/GFP (E), Muc5ac/GFP (G), Ki67/GFP (I) and Casp3/GFP (K). Scale bar equals 100 μm.

(B, D, F, H, J, L) $\Delta Np63^{\Delta/\Delta}$; $Rosa^{\Delta/\Delta}$ tracheal epithelium after polidocanol (PDO) treatment: H&E (B), Krt5/GFP (D), Ac-tub/GFP (F), Muc5ac/GFP (H), Ki67/GFP (J) and Casp3/GFP (K). Scale bar equals 100 μm.

(M) Quantification of staining for time point 2.

3.3 ΔNp63 is necessary for maintenance and differentiation of basal cells *in vitro*.

To further investigate the mechanism of ΔNp63 in maintenance of basal cells, we isolated basal cells from $\Delta Np63^{fl/fl}$; $Rosa^{M/M}$ mouse tracheas, cultured them *in vitro*, and infected the cells with either adeno-empty or adeno-cre to knock out ΔNp63. We found that $\Delta Np63^{\Delta/\Delta}$ basal cell colonies replicated *in vivo* proliferation patterns as early passage cells were more proliferative (Figure 12B) and late passage cells less proliferative compared to the wild type basal cells (Figure 12C). To investigate the effect of ΔNp63 loss on self-renewal, we cultured basal cells in a 3D medium. We found that the $\Delta Np63^{\Delta/\Delta}$ cells formed significantly fewer spheres (Figure 14D) that were also smaller in size (Figure 14E). The number and size of spheres formed by $\Delta Np63^{\Delta/\Delta}$ also decreased across passages. This effect was magnified by the passaging of the basal cells, as later passages of wild type basal cells exhibited increased sphere formation ability, suggesting a selection effect where a small percentage of wild type basal cells that were not infected by the adeno-cre outcompeted $\Delta Np63^{\Delta/\Delta}$ basal cells across multiple passages. To examine ΔNp63's role in basal cell differentiation, we differentiated basal cells in matrigel for 20 days (Rock et al., 2009). While the wild type basal cells formed hollow bi-layered spheres (Figure 15F and 15G) containing an outer layer of basal cells (Figure 15H) and an interior of ciliated and goblet cells (Figures 15J and 15K), $\Delta Np63^{\Delta/\Delta}$ basal cells formed smaller, mono-layered spheres (Figures 15L and 15M) that lacked staining for differentiation markers Ac-tub and Muc5ac. While the $\Delta Np63^{\Delta/\Delta}$ spheres lacked staining for basal cell marker Krt5 (Figure 15N), an alternative marker for basal cells NGFR was expressed (Figure 15O). Our data support a role of ΔNp63 in regulation of basal cell maintenance and differentiation.

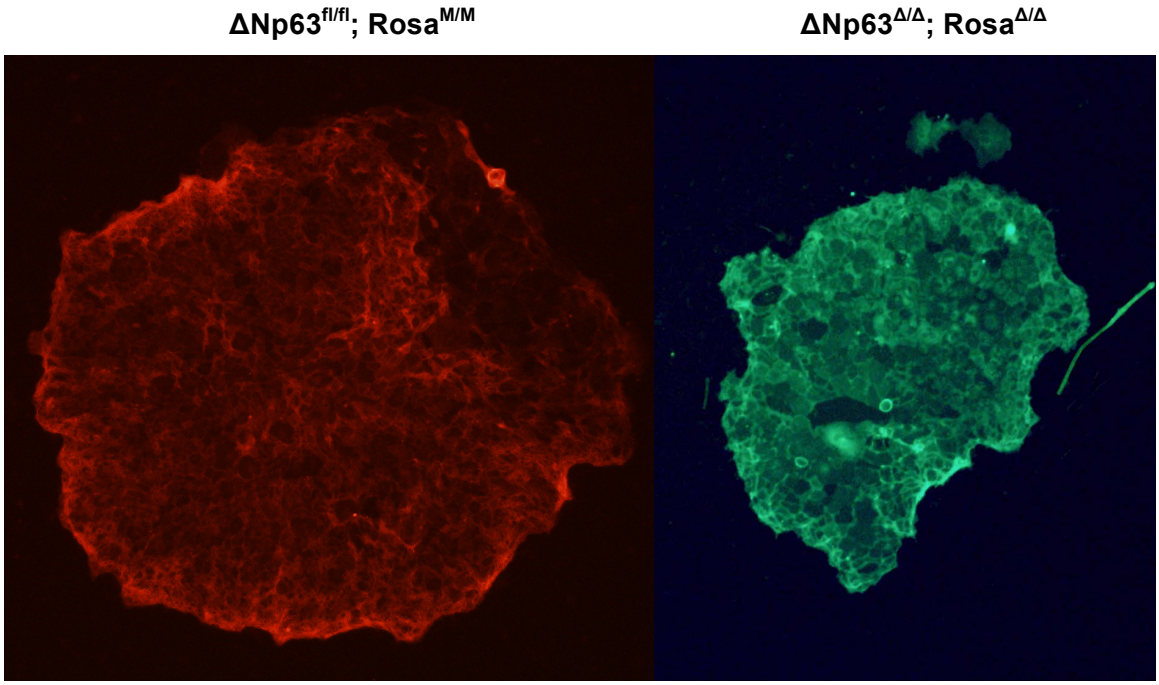

Figure 11. ΔNp63$^{Δ/Δ}$ basal cells form smaller colonies in 2D culture.

Basal cells isolated from mouse tracheal epithelium were infected with adenoviral-empty or adenoviral-cre and plated onto mitomycin-treated J2-3T3 feeders. ΔNp63$^{fl/fl}$ colonies (red fluorescence) were larger and more numerous than ΔNp63$^{Δ/Δ}$ colonies (green fluorescence).

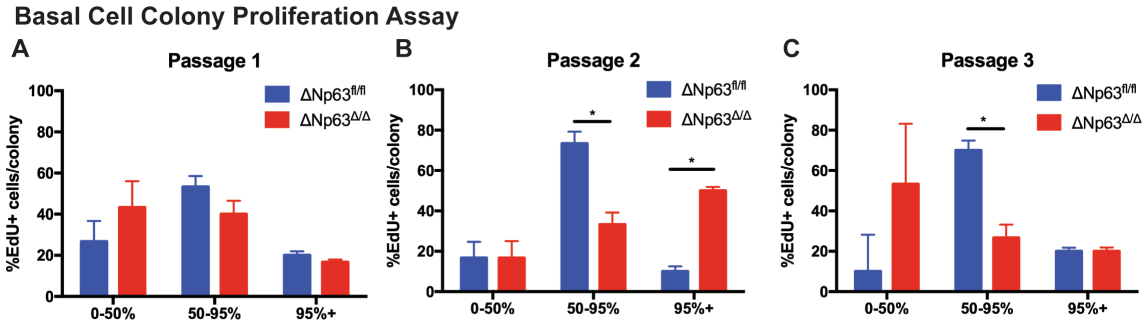

Figure 12. Basal cell colonies exhibit transient proliferative burst followed by decrease of proliferation after deletion of ΔNp63.

(A-C) EdU assay measuring proliferation of $\Delta Np63^{fl/fl}$ and $\Delta Np63^{\Delta/\Delta}$ colonies across passages 1 (A), 2 (B), and 3 (C).

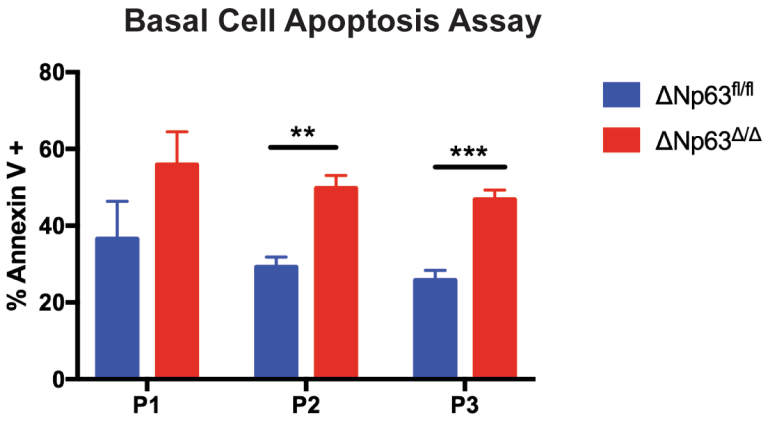

Figure 13. ΔNp63$^{Δ/Δ}$ basal cell colonies exhibit increased apoptosis.

Annexin V assay measuring apoptosis in ΔNp63$^{fl/fl}$ and ΔNp63$^{Δ/Δ}$ colonies across passages 1-3.

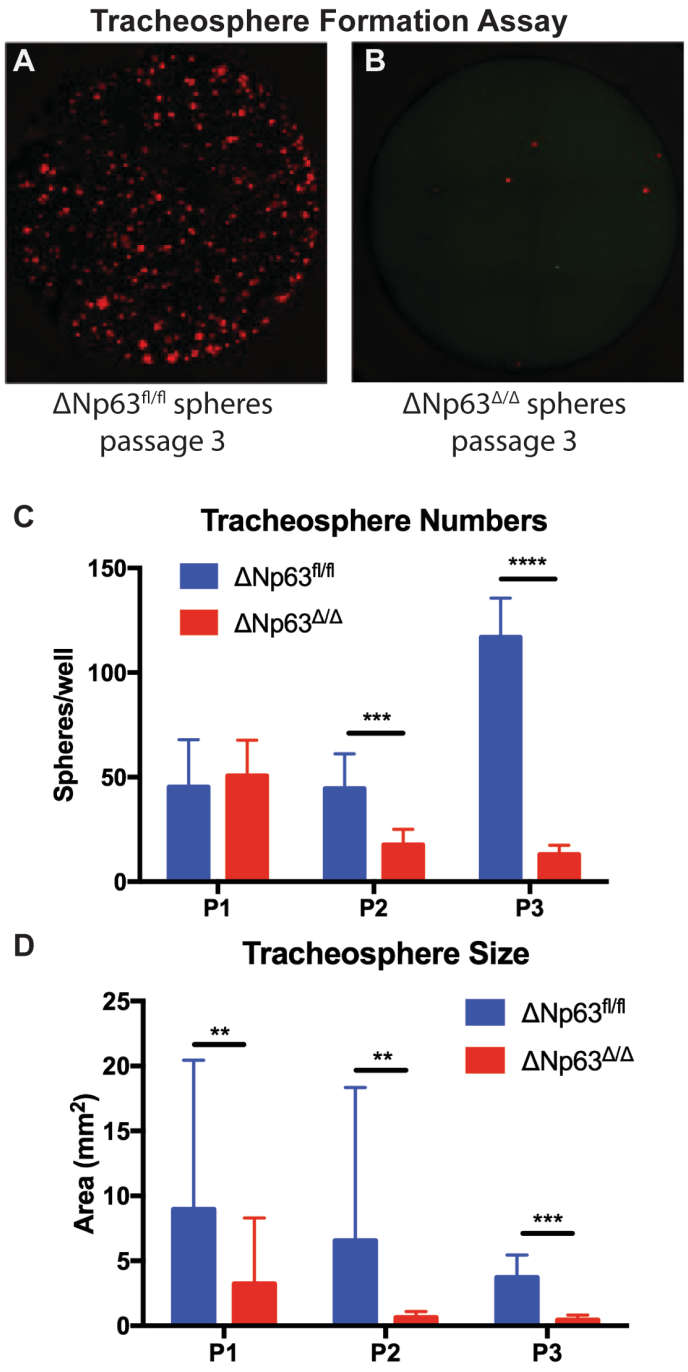

Figure 14. ΔNp63$^{Δ/Δ}$ basal cells have decreased sphere formation and sphere size.

(A, B) Representative wells of tracheosphere formation assay of ΔNp63$^{fl/fl}$ (A) and ΔNp63$^{Δ/Δ}$ (B) basal cells at passage 3.

(C, D) Tracheosphere formation assay (C) and tracheosphere size (D) of ΔNp63$^{fl/fl}$ and ΔNp63$^{Δ/Δ}$ basal cells across passages 1-3.

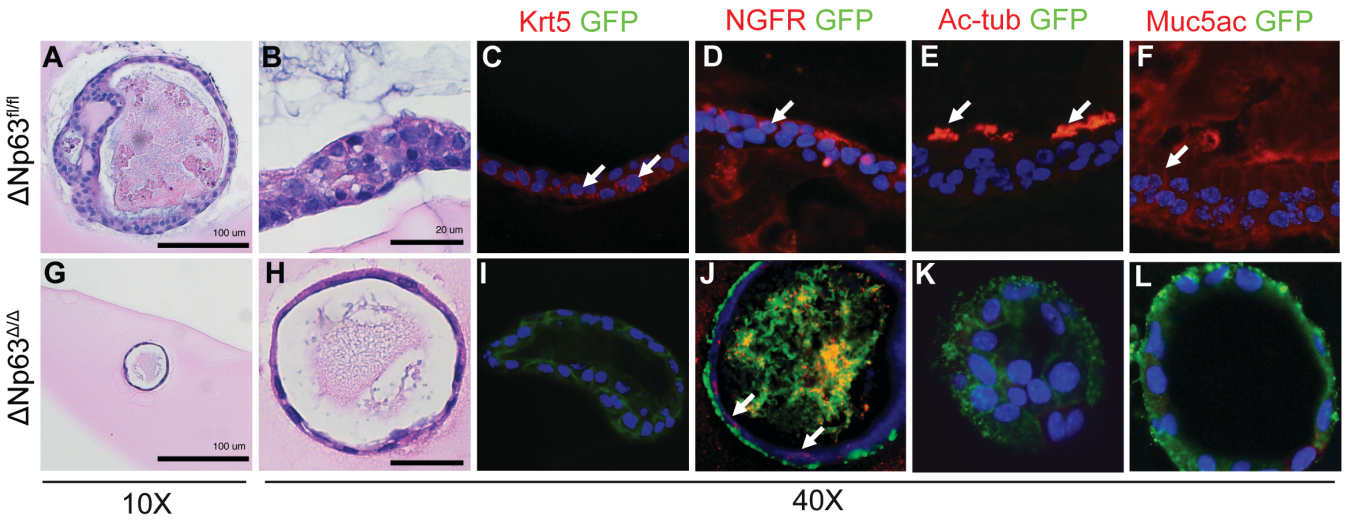

Figure 15. ΔNp63$^{Δ/Δ}$ tracheospheres have impaired ability to differentiate.

Tracheosphere differentiation assay for ΔNp63$^{fl/fl}$ and ΔNp63$^{Δ/Δ}$ basal cells: H&E (A and G), scale bar equals 100 um. H&E (B and H), Krt5/GFP (C and I), NGFR/GFP (D and J), Ac-tub/GFP (E and K), Muc5ac/GFP (F and L), scale bar equals 20 um.

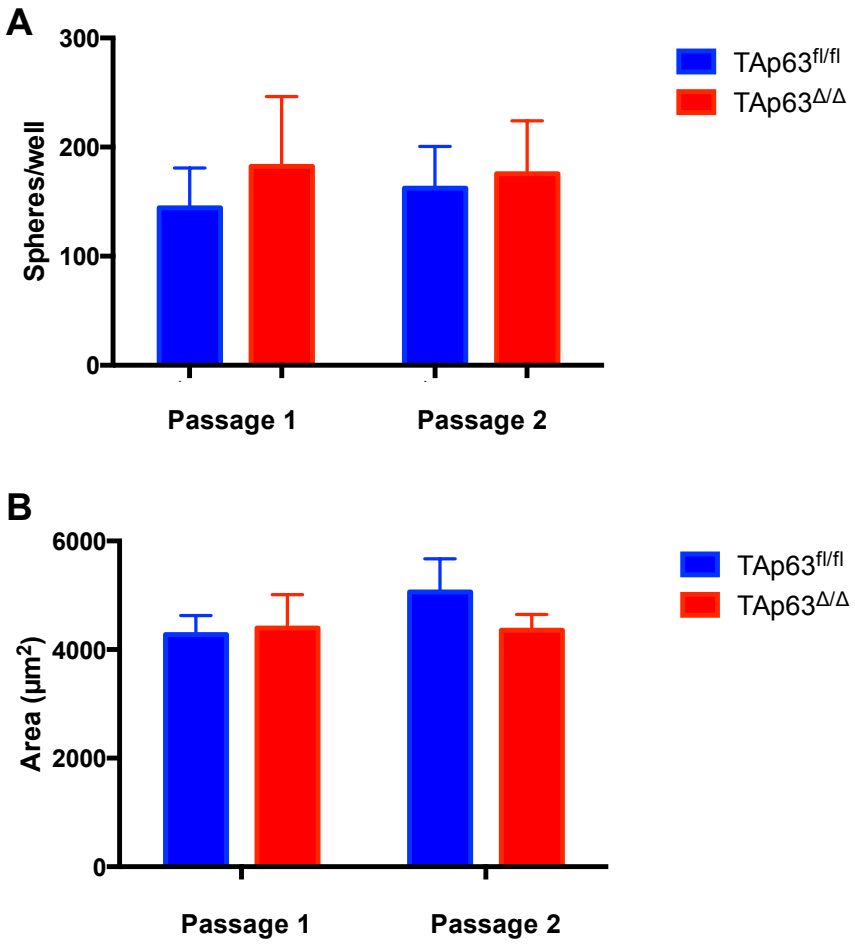

Figure 16. Differences in sphere formation numbers or size were not observed with TAp63$^{\Delta/\Delta}$ basal cells compared to wild type basal cells.

A. TAp63$^{\Delta/\Delta}$ basal cells sphere formation in 3D culture was not significantly changed compared to wild type basal cells.

B. TAp63$^{\Delta/\Delta}$ basal cells sphere size measured by area in 3D culture was not significantly changed compared to wild type basal cells.

3.4 ΔNp63 regulates cell identity genes in basal cells.

To further probe the transcriptional network of genes regulated by ΔNp63 in basal cells, we isolated basal cells to perform RNA-seq and ChIP-seq (Figure 17A). Basal cells from $\Delta Np63^{fl/fl}$; $Rosa^{M/M}$ mice were expanded on feeders, infected with either adeno-empty or adeno-cre, expanded again on feeders, and then collected for RNA-seq, miRNA-seq or ChIP-seq. Principle component analysis showed concordance between wild type and $\Delta Np63^{\Delta/\Delta}$ samples (Figure 18), as did generated heat maps for the RNA-seq and miRNA-seq (Figures 19 and 20). Ingenuity Pathway Analysis of the miRNA-seq data showed a network for genes regulated by upregulated and downregulated miRNAs (Figure 21). Pathway analysis in the RNA-seq data showed that major pathways affected after loss of ΔNp63 included those involved in proliferation, stem cell maintenance, and adhesion (Figure 17B). Genes involved in epithelialization and cell junction maintenance were downregulated in $\Delta Np63^{\Delta/\Delta}$ samples (Figure 17C). To characterize genome-wide ΔNp63 binding sites in this primary stem cell population, we utilized a method of perform low-cell number ChIP-seq. ChIP-seq using an antibody against p63 allowed us to generate a p63 binding motif that is similar to previously published p63 motifs (Figure 17D). The distribution of basal cell ChIP-seq peaks with regards to genomic features shows changes mostly in the intergenic and 10 kb upstream regions (Figure 22).

Recently, it has been shown that cell identify genes are often regulated by enhancers and super-enhancers which are marked by H3K27ac (Whyte et al., 2013, Loven et al., 2013). To determine the effect of ΔNp63 loss on enhancers and super-enhancers (a cluster of enhancers), we performed ChIP-seq for H3K27ac along with Pol2. Loss of ΔNp63 affected genome wide H3K27ac and Pol2 occupancy, especially at super-enhancers (Figures 23-27). ChIP-seq peaks showed that there was a loss of H3K27ac signal at *Krt5* and *BCL9L* after deletion of ΔNp63 (Figure 17F). Our data

indicate that ΔNp63 regulates basal cells through regulating transcription of super-enhancer associated cell identity genes.

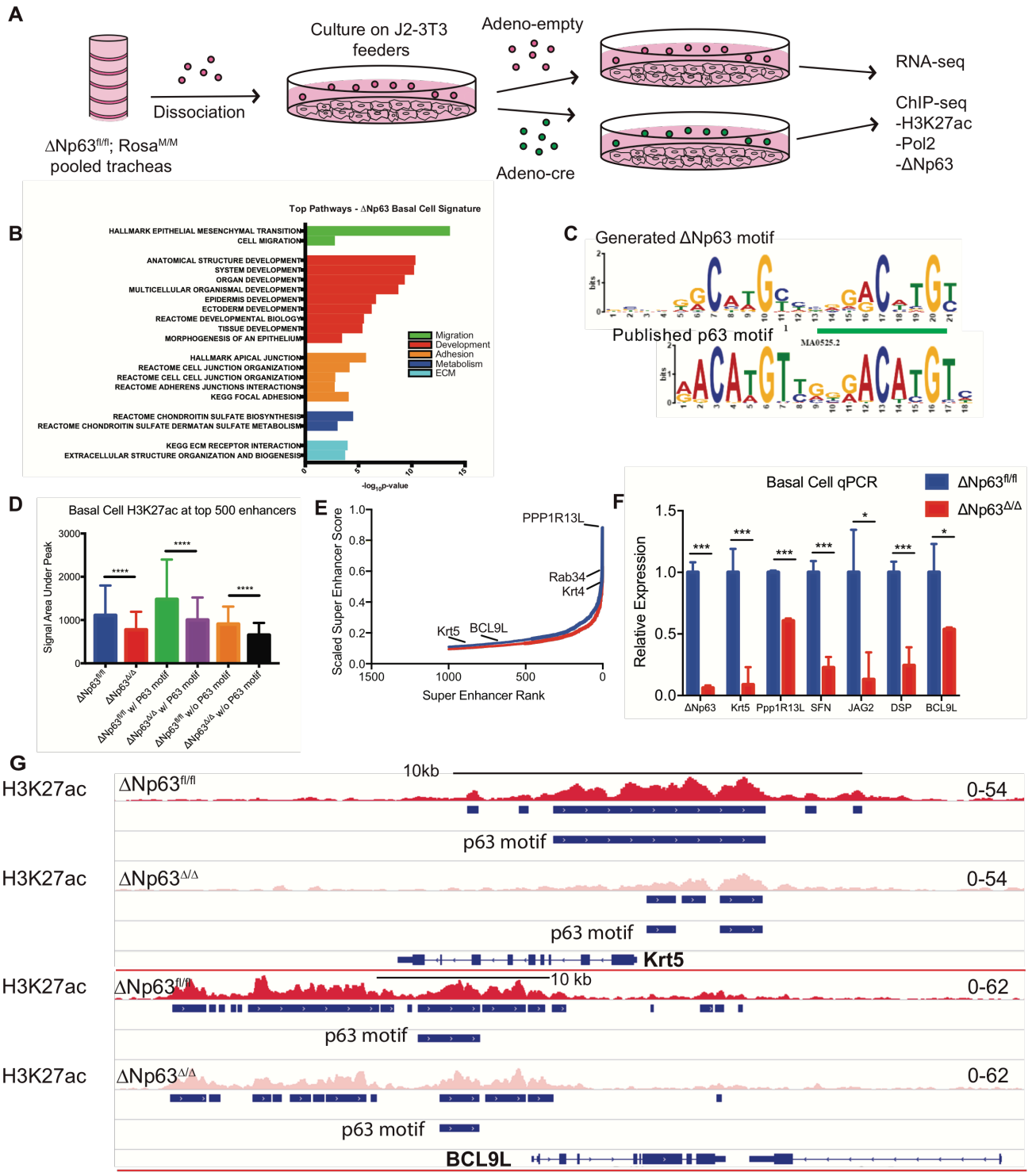

Figure 17. ΔNp63 regulates cell identity genes in basal cells.

(A) Schematic of isolation of ΔNp63$^{fl/fl}$ and ΔNp63$^{Δ/Δ}$ basal cells for RNA-seq and ChIP-seq.

(B) Pathway analysis of RNA-seq based on differentially expressed genes between ΔNp63$^{fl/fl}$ and ΔNp63$^{Δ/Δ}$ basal cells.

(C) qPCR validation of ΔNp63-regulated genes in basal cells.

(D) p63 motif derived from basal cell p63 ChIP-seq compared to published p63 motif.

(E) Super-enhancer curve based on H3K27ac ChIP-seq $\Delta Np63^{fl/fl}$ (blue) and $\Delta Np63^{\Delta/\Delta}$ (red) basal cells

(F) H3K27ac ChIP-seq signal area under peak for top 500 enhancers in basal cells.

(G) H3K27ac ChIP-seq signal area under peak for top 5000 enhancers in basal cells.

(H) ChIP-seq profiles for H3K27ac in $\Delta Np63^{fl/fl}$ (red) and $\Delta Np63^{\Delta/\Delta}$ (pink) basal cells for genes *Krt5* and *BCL9L*.

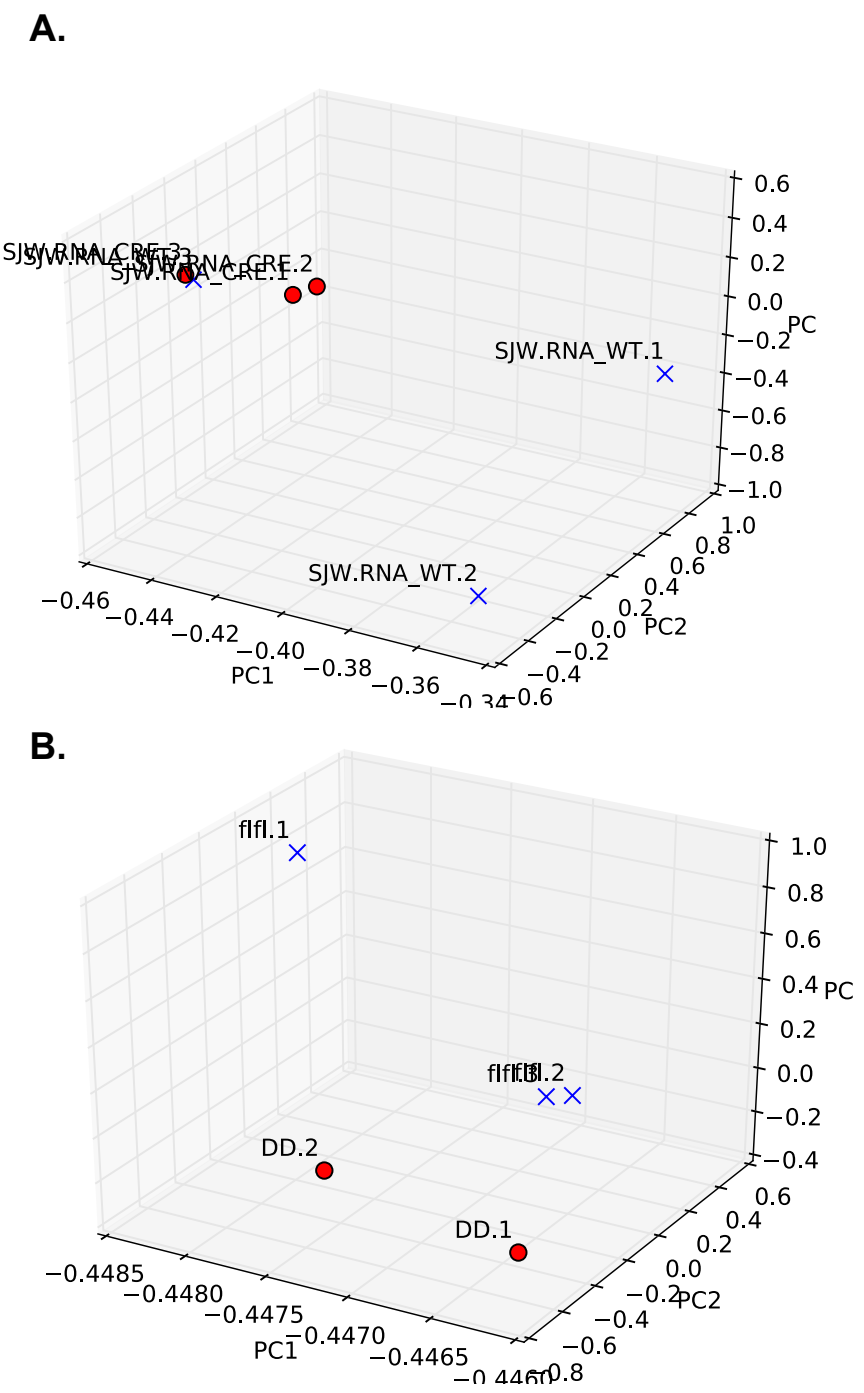

Figure 18: PCA analysis of RNA-seq and miRNA-seq samples for basal cells.

Principle component analysis (PCA) of basal cell RNA-seq (A) demonstrates clustering of ΔNp63$^{\Delta/\Delta}$ samples (SJW.RNA_CRE.1-3) compared to ΔNp63$^{fl/fl}$ samples. miRNA-seq (B) PCA of ΔNp63$^{fl/}$fl(flfl) and ΔNp63$^{\Delta/\Delta}$(DD) samples.

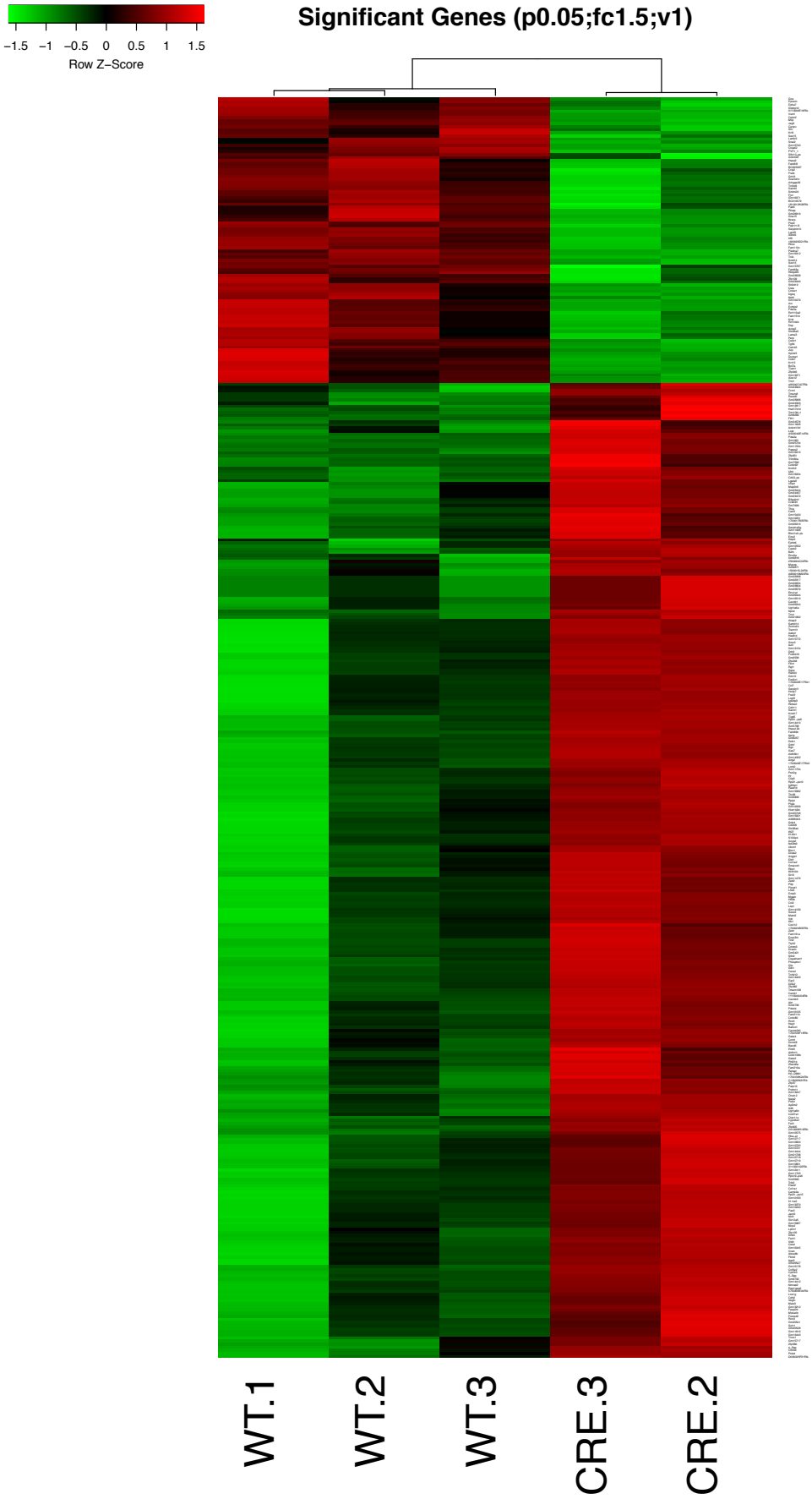

Figure 19. Heat map of RNA-seq from ΔNp63$^{fl/fl}$ and ΔNp63$^{Δ/Δ}$ basal cells.

Differential gene expression of downregulated (red) and upregulated (green) genes of ΔNp63$^{fl/fl}$(WT) and ΔNp63$^{Δ/Δ}$(CRE) basal cells.

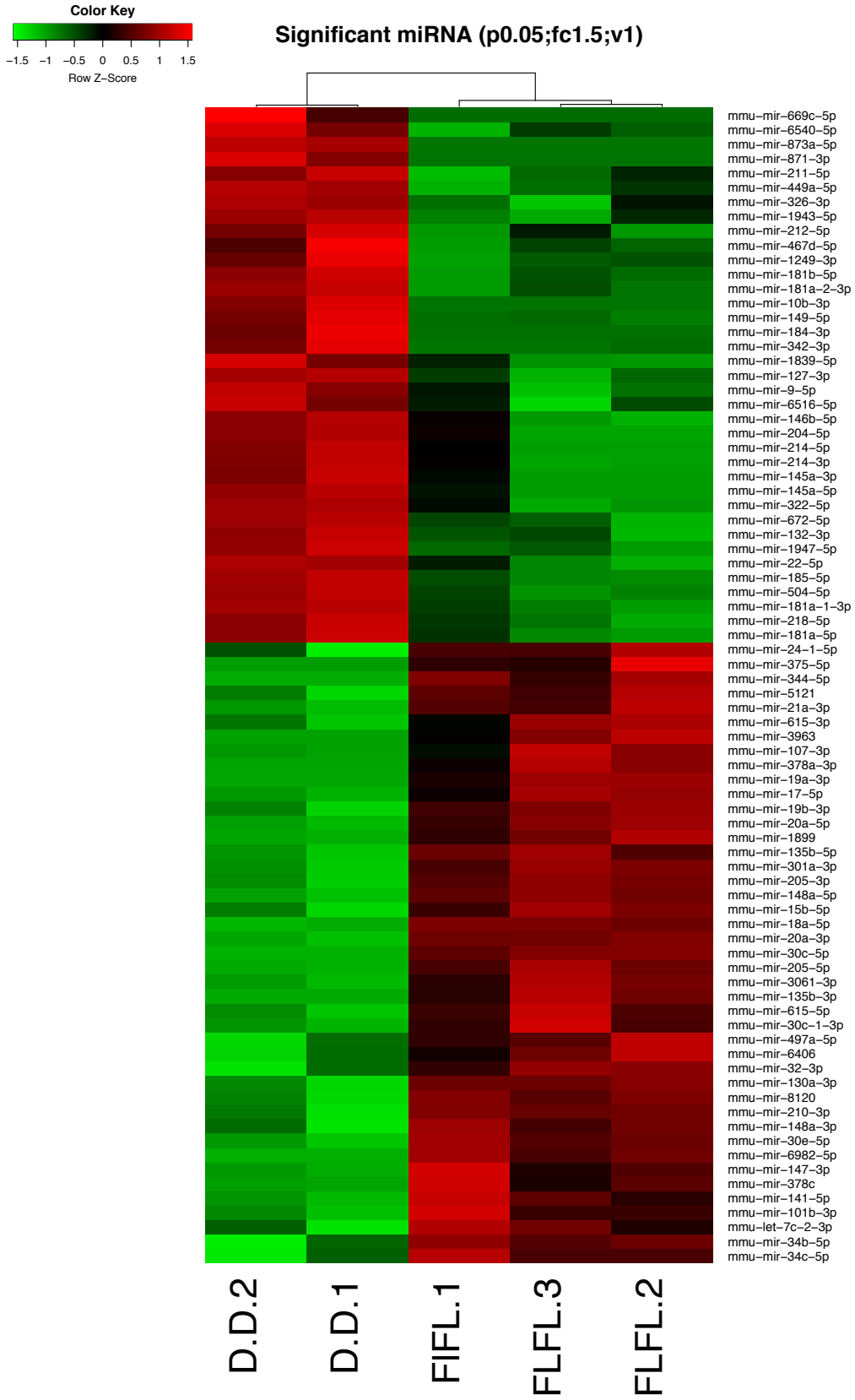

Figure 20. Heat map of miRNA-seq from ΔNp63$^{fl/fl}$ and ΔNp63$^{Δ/Δ}$ basal cells.

Differential gene expression of downregulated (red) and upregulated (green) genes of ΔNp63$^{fl/fl}$(FLFL) and ΔNp63$^{Δ/Δ}$(D.D.) basal cells.

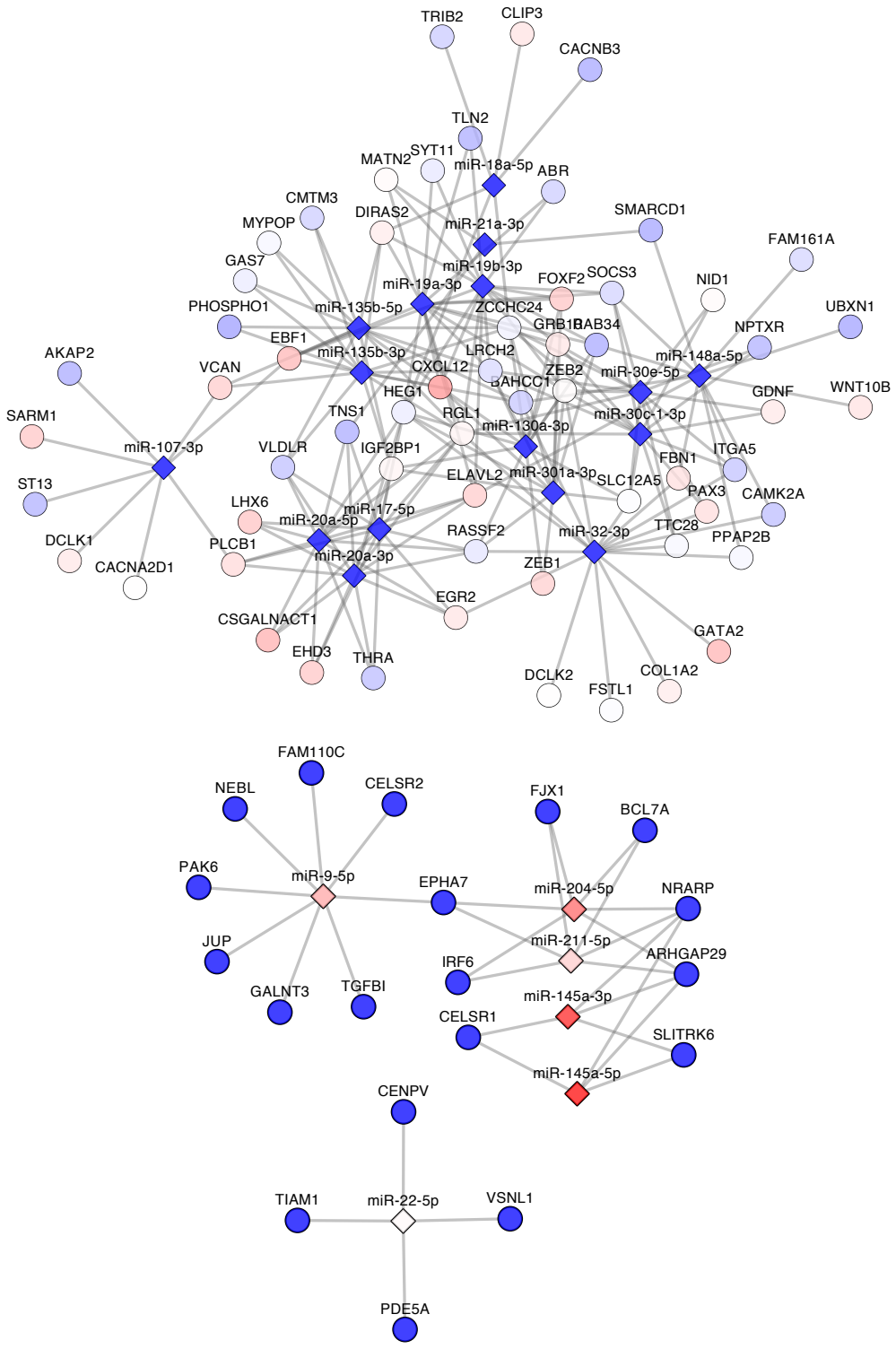

Figure 21. ΔNp63 controls miRNA-mRNA network of basal cells.

Pathway analysis of genes regulated by ΔNp63-regulated miRNAs.

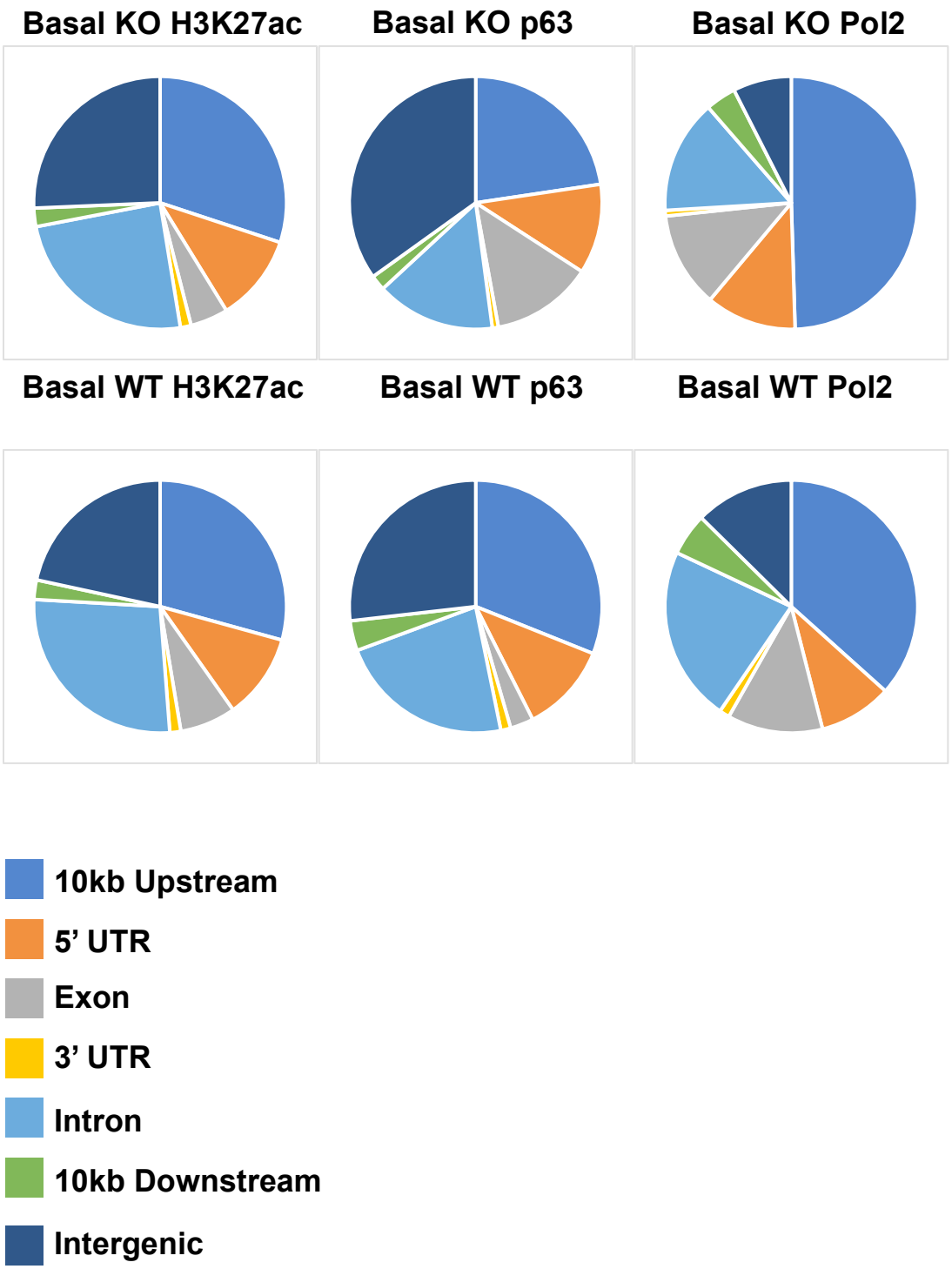

Figure 22. Distribution of basal cell ChIP-seq peaks with regards to genomic features.

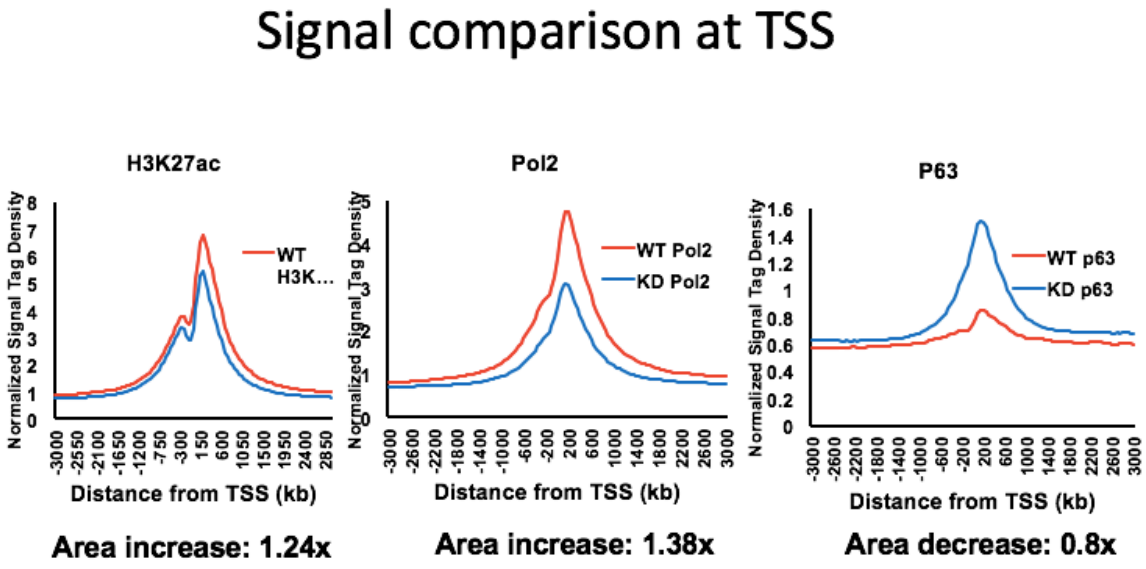

Figure 23. Signal comparison at the transcription start site (TSS) for ΔNp63 wild type and knockout basal cells.

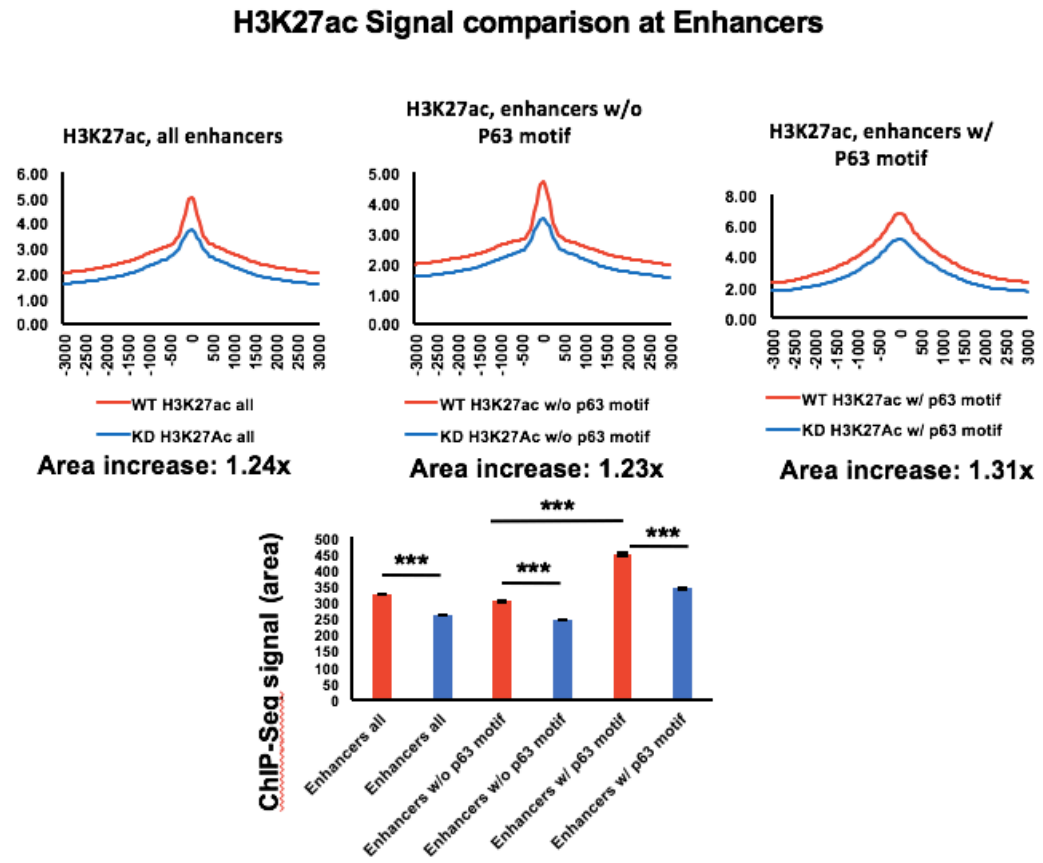

Figure 24. Signal comparison of H3K27ac ChIP-seq at enhancers for ΔNp63 wild type and knockout basal cells.

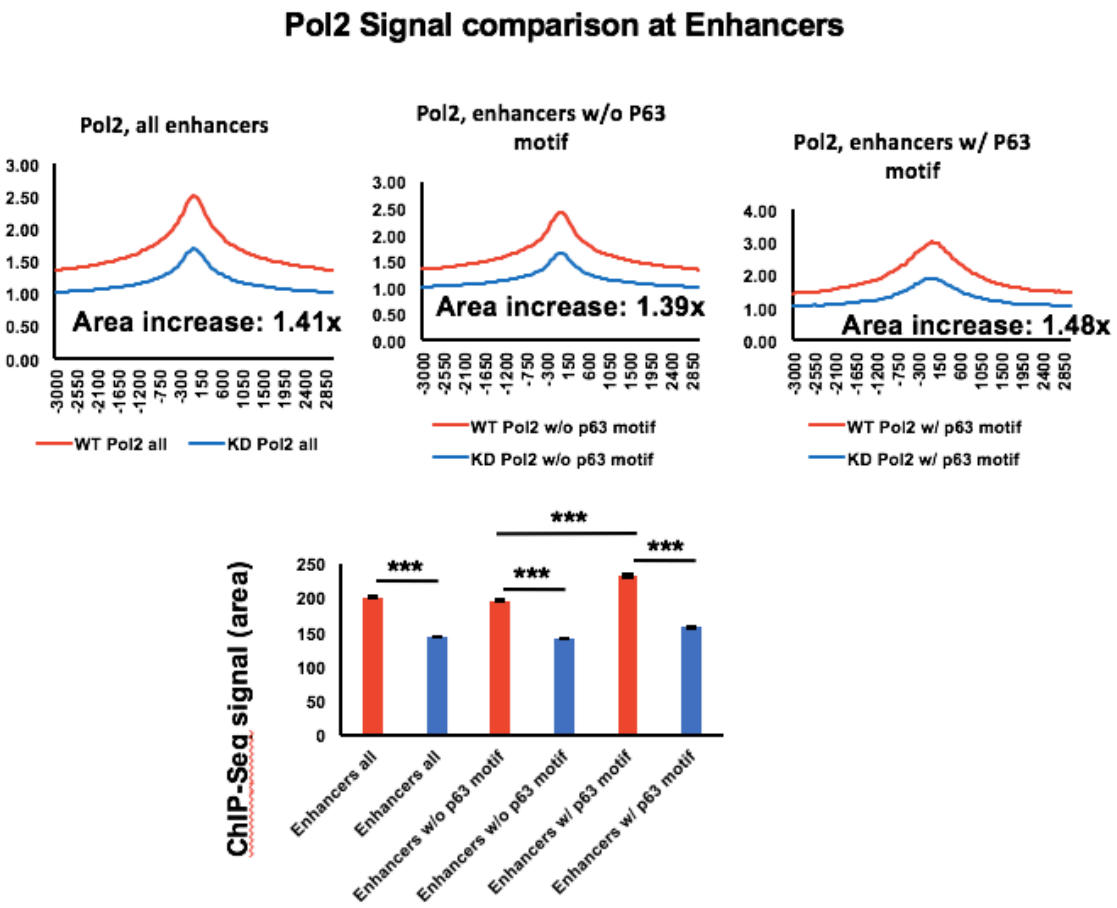

Figure 25. Signal comparison of Pol2 ChIP-seq at enhancers for ΔNp63 wild type and knockout basal cells.

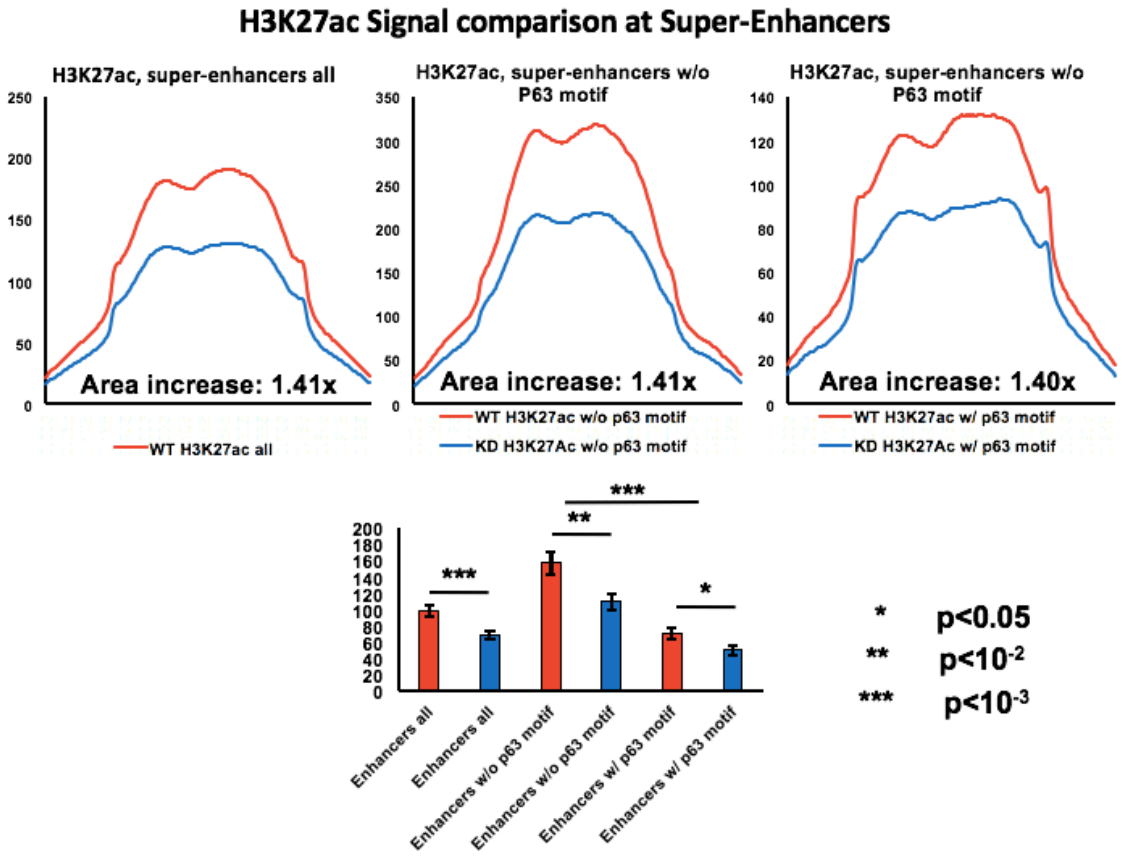

Figure 26. Signal comparison of H3K27ac ChIP-seq at super-enhancers for ΔNp63 wild type and knockout basal cells.

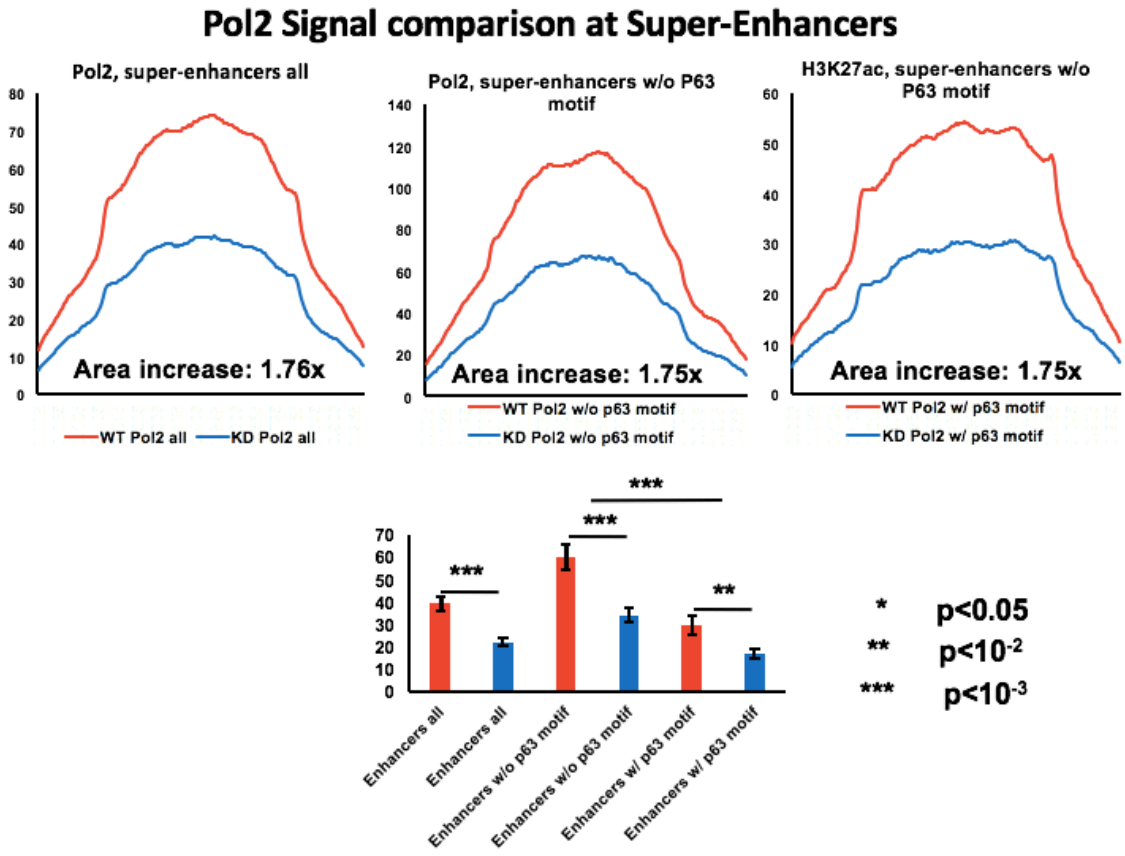

Figure 27. Signal comparison of Pol2 ChIP-seq at super-enhancers for ΔNp63 wild type and knockout basal cells.

4. Chapter 4: Functions of p63 isoforms in stem cells of the distal lung.

Chapter 4: Functions of p63 isoforms in stem cells of the distal lung.

To profile the role of ΔNp63 in the distal lung, we profiled the lungs of $\Delta Np63^{fl/fl}$; $Rosa^{M/M}$ and $\Delta Np63^{\Delta/\Delta}$; $Rosa^{M/M}$ mice for AT2 cell marker SPC. Though we observed slight increases of SPC+ cells at 1 month and decreases at 3 months in the ΔNp63 ad-cre treated mice, the changes were not significantly different (Figure 28).

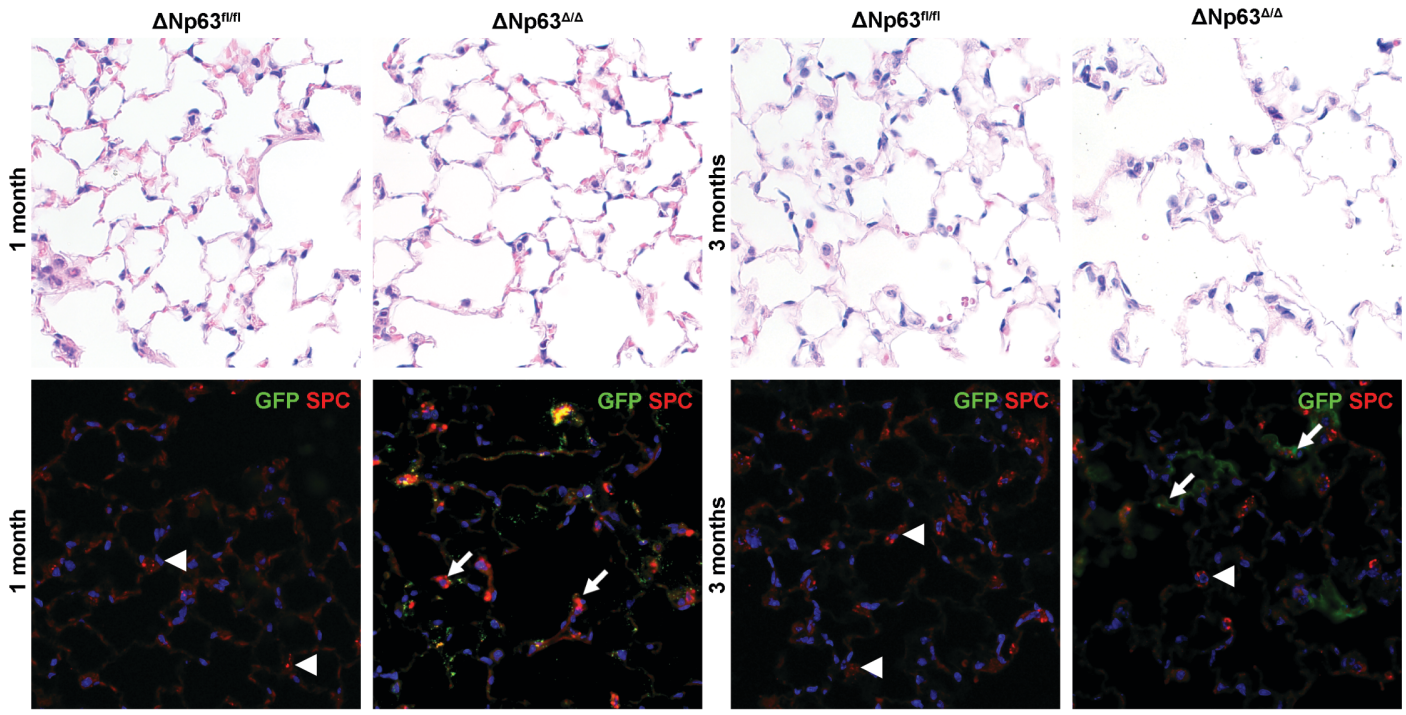

Figure 28. Distal lung shows few differences between ΔNp63$^{fl/fl}$; Rosa$^{M/M}$ and ΔNp63$^{Δ/Δ}$; Rosa$^{Δ/Δ}$ distal lung 1 and 3 months post-induction

ΔNp63$^{fl/fl}$; Rosa$^{M/M}$ and ΔNp63$^{Δ/Δ}$; Rosa$^{Δ/Δ}$ lung 1 and 3 months post-induction: H&E and SPC/GFP. Add Scale bar equals 100 μm.

As we observed a role of ΔNp63 in initiation of lung adenocarcinoma, we also aimed to profile distal lung stem cells. We also isolated AT2 and BASC cells from $\Delta Np63^{fl/fl}$; $Rosa^{M/M}$ (Figure 29A). In a colony formation assay, $\Delta Np63^{-/-}$ AT2 and BASC exhibited decreased colony formation (Figure 29B and 29C). To determine the effect of ΔNp63 loss in regulating enhancers and super-enhancers, we performed H3K27ac ChIP-seq in AT2 cells from $\Delta Np63^{fl/fl}$; $Rosa^{M/M}$ mice. Similar to basal cells, ChIP-seq for H3K27ac also showed a global decrease of marks after loss of ΔNp63 (Figure 29D and 29E). Ranking of genes based on H3K27ac signal identified super-enhancer associated genes in AT2 cells that had decreased expression after loss of ΔNp63 (Figure 29F and 29G). ETV5 was recently identified as an essential gene for maintenance of the AT2 cell population and was identified in our analysis as significantly decreased after loss of ΔNp63. ChIP-seq peaks show that there is a loss of H3K27ac signal at *ETV5* and *BCL9L* after deletion of ΔNp63 (Figure 29H and 30). Our results suggest that ΔNp63 also regulates cell identity gene expression in the distal lung stem cell population.

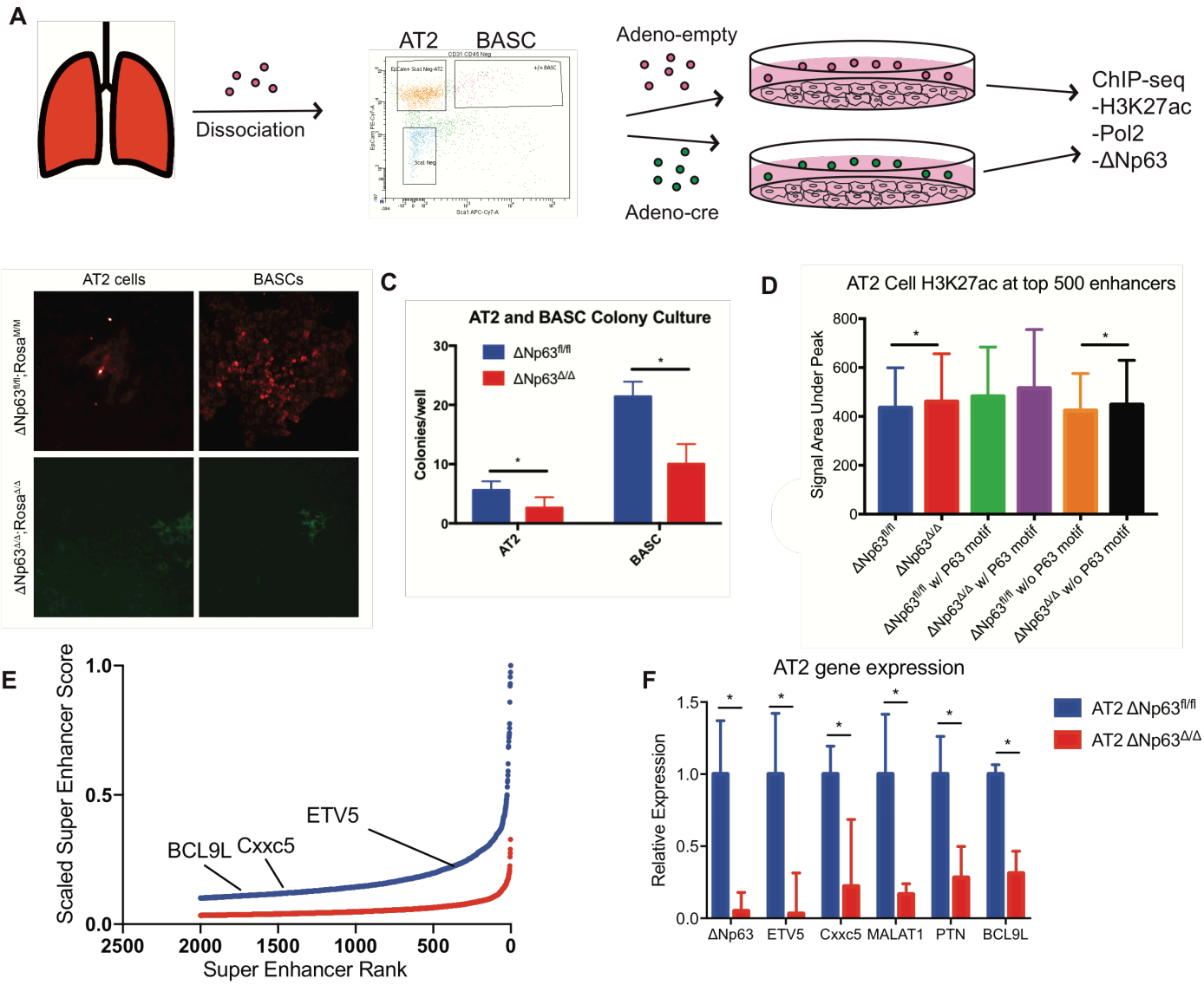
A
Dissociation
AT2
BASC
Adeno-empty
Adeno-cre
ChIP-seq
-H3K27ac
-Pol2
-ΔNp63
B
AT2 cells
BASCs
ΔNp63fl/fl;RosaM/M
ΔNp63Δ/Δ;RosaΔ/Δ
C
AT2 and BASC Colony Culture
ΔNp63fl/fl
ΔNp63Δ/Δ
Colonies/well
AT2
BASC
D
AT2 Cell H3K27ac at top 500 enhancers
Signal Area Under Peak
ΔNp63fl/fl
ΔNp63Δ/Δ
ΔNp63fl/fl w/ P63 motif
ΔNp63Δ/Δ w/ P63 motif
ΔNp63fl/fl w/o P63 motif
ΔNp63Δ/Δ w/o P63 motif
E
Scaled Super Enhancer Score
Super Enhancer Rank
ETV5
BCL9L
Cxxc5
F
AT2 gene expression
Relative Expression
AT2 ΔNp63fl/fl
AT2 ΔNp63Δ/Δ
ΔNp63
ETV5
Cxxc5
MALAT1
PTN
BCL9L
G
H3K27ac
ΔNp63fl/fl
ΔNp63Δ/Δ
10 kb
0-2.69
ETV5
0-3
p63 motif
BCL9L

Figure 29. ΔNp63 regulates stemness in distal lung stem cells.

(A) Schematic of isolation of $\Delta Np63^{fl/fl}$ and $\Delta Np63^{\Delta/\Delta}$ AT2 cells and BASC cells for RNA-seq and ChIP-seq.

(B-C) Colony formation assay for $\Delta Np63^{fl/fl}$ and $\Delta Np63^{\Delta/\Delta}$ AT2 cells and BASCs (B) with quantification (C).

(D-E) Signal histogram for $\Delta Np63^{fl/fl}$ and $\Delta Np63^{\Delta/\Delta}$ AT2 cell H3K27ac ChIP-seq (D) with calculation of area under the curve (E).

(F) Super-enhancer curve based on H3K27ac ChIP-seq $\Delta Np63^{fl/fl}$ (blue) and $\Delta Np63^{\Delta/\Delta}$ (red) AT2 cells

(G) qPCR validation of ΔNp63-regulated genes in AT2 cells.

(J) ChIP-seq profiles for H3K27ac in $\Delta Np63^{fl/fl}$ (red) and $\Delta Np63^{\Delta/\Delta}$ (pink) AT2 cells for genes *ETV5* and *BCL9L*.

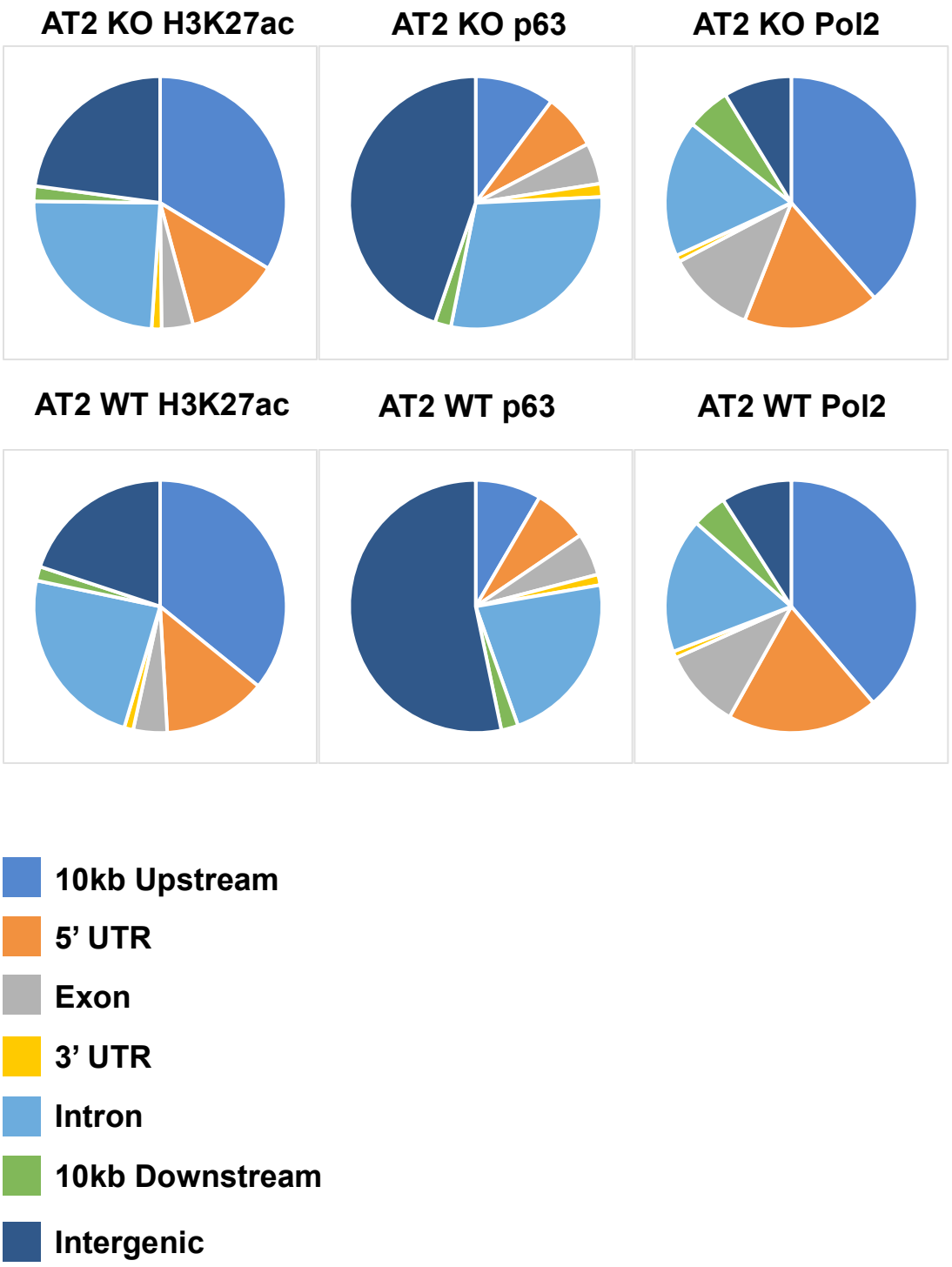

Figure 30. Distribution of AT2 cell ChIP-seq peaks with regards to genomic features.

5. Chapter 5: ΔNp63 in lung tumorigenesis.

Chapter 5: ΔNp63 in lung tumorigenesis.

Our lab recently utilized a keratinocyte-derived signature of ΔNp63-regulated genes to assign a putative oncogenic role to ΔNp63 in the context of lung squamous cell carcinoma (LUSC) and lung adenocarcinoma (LUAD)(Abbas et al., 2018). The designation of ΔNp63 as an oncogene in LUSC was not surprising, as ΔNp63 is highly amplified in LUSC (Cancer Genome Atlas Research, 2012) and has been utilized as a positive diagnostic marker for LUSC (Conde et al., 2010). However not much is known about ΔNp63's role in LUAD, as ΔNp63 is often used as a negative marker for the diagnosis of LUAD. To interrogate whether ΔNp63 functions as an oncogene in the context of LUSC, we utilized shRNAs to knock down ΔNp63 in human LUSC cell lines H520 and H2170. To determine the effect of ΔNp63 on anchorage-independent growth, H520 and H2170 cell lines were grown in a soft agar assay. H520 and H2170 stably transfected with shΔNp63 formed significantly fewer colonies than shControl cell lines (Figures 31C and 31D). H520 and H2170 shΔNp63 cell lines also formed significantly smaller flank tumors in xenograft mice compared to shControl cell lines (Figures 31A and 31B), with almost complete absence of tumor formation in the H2170 shΔNp63 cell line, demonstrating a potent ability for ΔNp63 inhibition to decrease tumor growth *in vivo*. ΔNp63 knockdown tumors had decreased proliferation (Figures 31F and 31J) and increased staining for apoptotic marker cleaved caspase-3 (Figures 31H and 31L). Our data support ΔNp63's oncogenic role in the context of LUSC through maintenance of anchorage independent growth and inhibition of cell death.

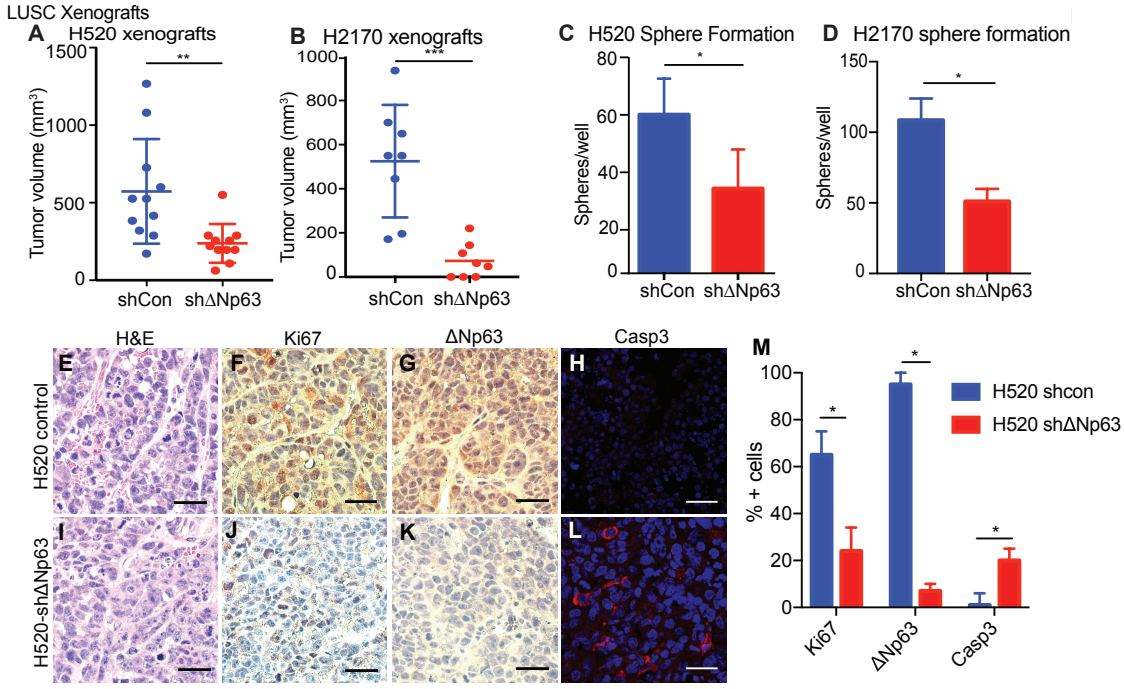

Figure 31. ΔNp63 promotes tumor initiation and progression in human lung squamous cell carcinoma cell line.

(A and B) Comparison of colony formation in soft agar of LUSC cell line (A) H520 shControl and shΔNp63 and (B) H2170 shControl and shΔNp63.

(C and D) Comparison of tumor volume of xenografted LUSC cell line (C) H520 shControl and shΔNp63 (n=11) and (D) H2170 shControl and shΔNp63 (n=8).

(E-L) Representative images of xenograft tumors for H520 shControl and shΔNp63 for H&E (E and I), Ki67 (F and J), ΔNp63 (G and K), and Casp3 (H and L). Scale bar equals 100 μm.

(M) Quantification of immunohistochemical staining for Figure 1 F-H and J-L.

To determine the role of ΔNp63 in lung adenocarcinoma, we generated a new mouse model by crossing the LSLKras^{G12D} mouse to the ΔNp63 conditional knockout mouse (Chakravarti et al., 2014) and inducing recombination through intratracheal administration of adenoviral Cre recombinase (DuPage et al., 2009) with robust recombination efficiency in the trachea and lung parenchyma. When examining a time point of 20 weeks post-induction with adenoviral cre, Lox-Kras^{G12D} mice formed lung adenomas as previously reported (Jackson et al., 2001) (Figure 32A). In comparison, the lungs in compound ΔNp63$^{\Delta/\Delta}$; Lox-Kras^{G12D} mice had a significant decrease of lung adenoma formation (Figure 32A). Examination and grading of the lung lesions(Jackson et al., 2001) revealed significantly fewer lesions of all grades (atypical adenomatous hyperplastic lesions, grade 1, grade 2+) in ΔNp63$^{\Delta/\Delta}$; Lox-Kras^{G12D} mice compared to Lox-Kras^{G12D} mice (Figure 32B). Interestingly, tumors from Lox-Kras^{G12D} mice stained positive for ΔNp63 while ΔNp63$^{\Delta/\Delta}$; Lox-Kras^{G12D} lesions were negative (Figures 32E and 32F). Non-tumorigenic lung epithelium does not have detectable levels of ΔNp63, suggesting the increase may be a result of activation from the mutant Kras driver.

We also investigated how ΔNp63 and TAp63 could affect tumorigenesis of mutant p53 driven cancer. We crossed the ΔNp63fl/fl and TAp63fl/fl mice with LSLp53R172H/+ mice and observed a general decrease of tumorigenesis of grade 2+ lung lesions but no significant difference in AAH or grade 1 lesions (Figure 33).

Our results provided evidence for an unexpected role of ΔNp63 in the initiation and development of lung adenocarcinoma lesions.

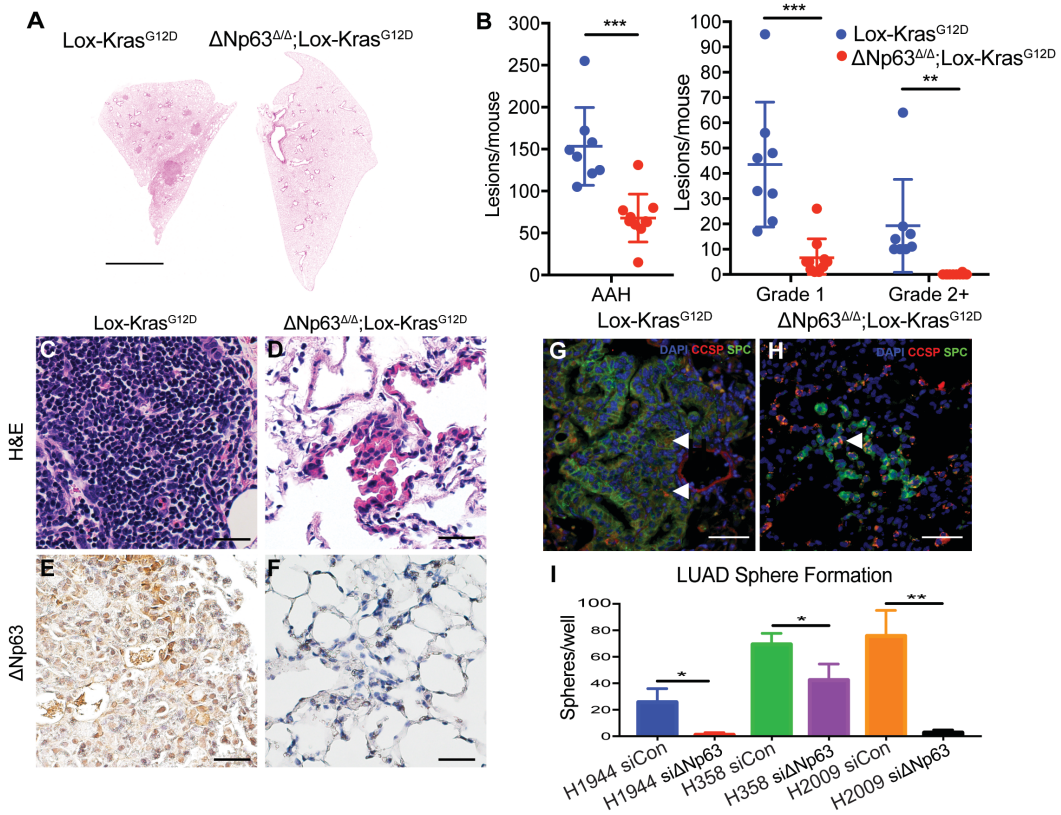

Figure 32. ΔNp63 promotes tumor initiation and progression in a mouse model of lung adenocarcinoma.

(A) Representative lung lobes from Lox-Kraxs^{G12D} and ΔNp63Δ/Δ; Lox-Kras^{G12D} mice. Scale bar equals 3 mm.

(B) Lung tumor grading of Lox-Kras^{G12D} and ΔNp63$^{Δ/Δ}$; Lox-Kras^{G12D} mice grouped by lesions per mouse for categories of atypical adenomatous hyperplasia (AAH), Grade 1, and Grade 2+.

(C-F) Representative images of lung lesions from Lox-Kras^{G12D} and ΔNp63$^{Δ/Δ}$; Lox-Kras^{G12D} mouse: H&E (P and Q) and ΔNp63 (R and S) respectively. Scale bar equals 100 μm.

(G and H) Representative staining for CCSP and SPC in lung adenoma from Lox-Kras^{G12D} mouse (T) and ΔNp63$^{Δ/Δ}$; Lox-Kras^{G12D} mouse (U). Scale bar equals 100 μm.

(I) Soft agar assay in LUAD cell lines H1944, H358, and H2009 with siControl and siΔNp63 knockdown.

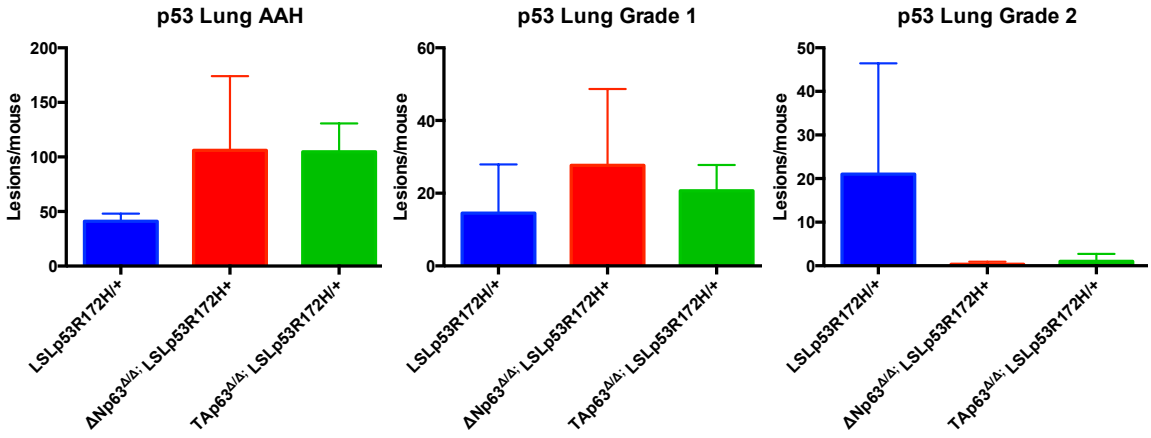

Figure 33. Tumor spectrum of LSLp53R172H/+ mice crossed with p63 isoform conditional knockout mice.

Analysis of lungs from LSLp53R172H/+, ΔNp63$^{\Delta/\Delta}$; LSLp53R172H/+, and TAp63$^{\Delta/\Delta}$; LSLp53R172H/+ scored for atypical adenomatous hyperplasia (AAH), grade 1 and grade 2+ lesions.

6. Chapter 6: Epigenetic mechanisms of ΔNp63 in tumorigenesis

Chapter 6: Epigenetic mechanisms of ΔNp63 in tumorigenesis

ΔNp63 coordinates with p300 to regulate oncogenic super-enhancer associated genes in human cancer cell lines.

After analyzing the super-enhancer signatures from AT2 cells and basal cells, we found a list of AT2-specific, basal-specific, and common genes regulated by ΔNp63 (Figure 34A). To enable translation into human samples, we cross-referenced the identified genes with H3K27ac ChIP-seq data from human lung cancer cell lines. We located super-enhancers in each of these data sets and identified genes located near super-enhancer regions, which also contained a p63-binding motif. Genes that met these criteria were crosschecked with the LUAD and LUSC TCGA databases for alterations in cancer. As we hypothesized ΔNp63's primary contribution to tumorigenesis as through maintenance of stem cell renewal and differentiation pathways, we focused on genes that were reported to have functions in stem cell biology. In the end, we focused on Krt5 as the basal cell specific gene, ETV5 as the AT2 specific gene, and BCL9L as the common gene.

To determine whether ΔNp63 regulates super-enhancers, we co-targeted ΔNp63 and the histone acetyltransferase p300 to several super-enhancer regions in which H3K27ac signals were reduced by ΔNp63 by employing a deactivated Cas9 (dCas9) targeting strategy (ref). We transfected 293T cells with vectors expressing dCas9-conjugated proteins p300 and ΔNp63 to target these proteins to super-enhancer regions with a p63 motif (Figure 34B). In addition, we co-transfected 4 sgRNAs per region of super-enhancers for Krt5, ETV5, and BCL9L into 293T cells. We found that while dCas9-p300 alone had no significant effect on gene expression. dCas9-ΔNp63 recruitment to a super-enhancer p63 motif significantly increased gene expression (Figures 34C-34E).

The combination of dCas9-ΔNp63 and dCas9-p300 recruitment further increased gene expression significantly over dCas9-ΔNp63 alone, demonstrating an additive effect of ΔNp63 and p300 to induce gene expression.

To ask whether ΔNp63 and p300 co-localize at p63 motifs located in super-enhancer regions, we performed chromatin immunoprecipitation in the H520 cell line which expresses high levels of ΔNp63, comparing shcontrol and shΔNp63 cell lines. We found that occupancy levels of H3K27ac, p300 and ΔNp63 at ETV5, BCL9L, and Krt5 genes significantly decreased in shΔNp63 cells compared to shControl cells (Figures 34F-34H), supporting a mechanism for ΔNp63 and p300 co-recruitment at p63 motifs to promote histone acetylation in enhancer regions.

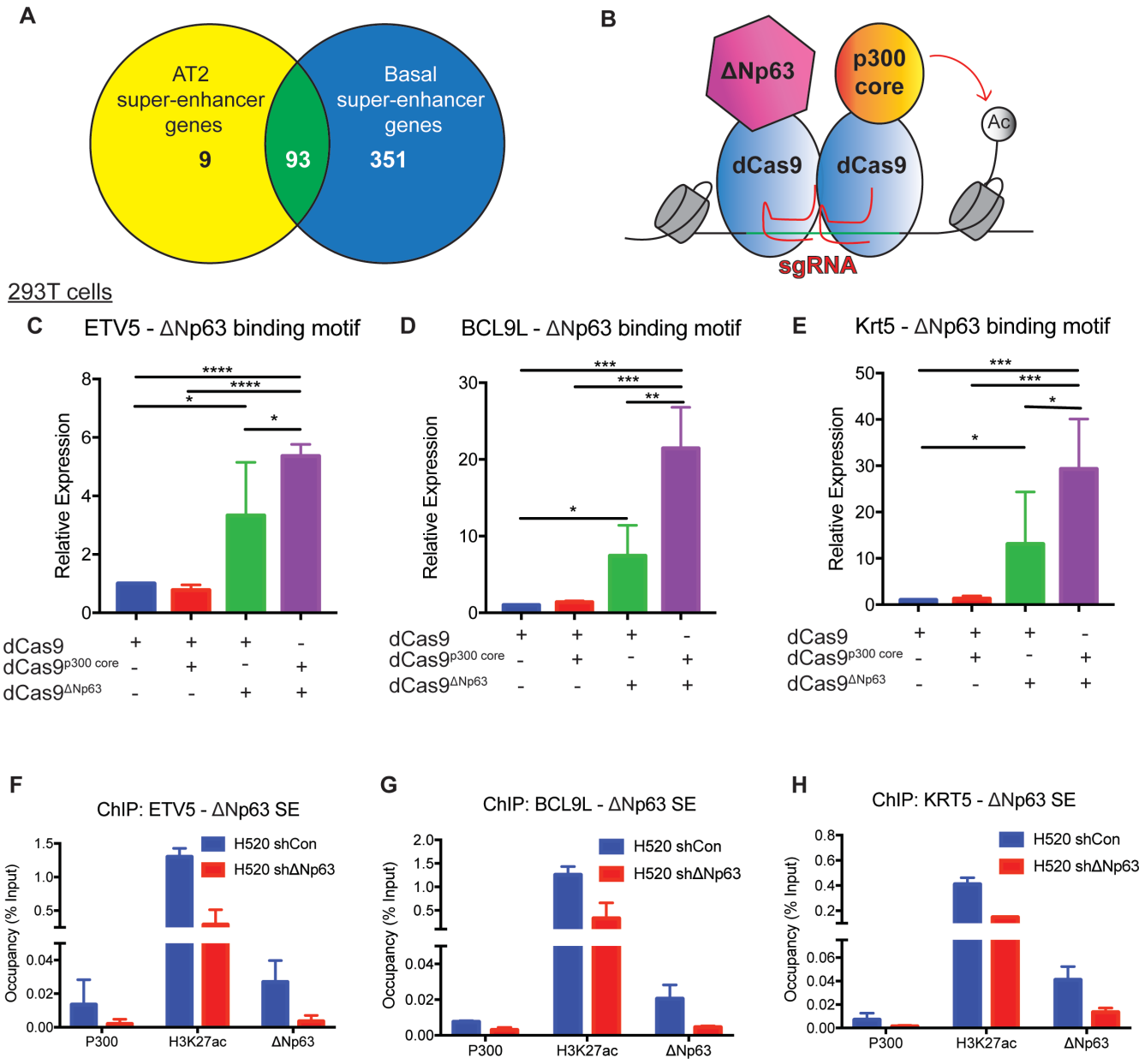

Figure 34. ΔNp63 coordinates with p300 to regulate oncogenic super-enhancer associated genes in human cancer cell lines.

(A) Venn diagram overlaying ΔNp63-regulated super-enhancer associated genes in AT2 cells and basal cells.

(B) Schematic of dCas9-p300 and dCas9-ΔNp63 sgRNA experiment.

(C-E) Relative change in gene expression at the p63 binding motif of *ETV5* (C), *BCL9L* (D), *and KRT5* (E) genes in 293T cells after transfection with dCas9 elements.

(F-H) Quantitative ChIP assay in H520 shControl and shΔNp63 cells for p300, H3K27ac, and ΔNp63 occupancy at the p63 motif of genes *ETV5* (F), *BCL9L* (G), and *Krt5* (H).

To understand the functional roles of these genes, we used shRNA to knockdown expression of *BCL9L*, *KRT5*, and *ETV5* in LUSC cell line H520 and LUAD cell line H358 (Figure 35). In an in vitro soft agar assay, we found that knocking down common gene *BCL9L* and basal cell gene *Krt5* significantly reduced colony formation in LUSC cell line H520, whereas knock down of AT2 cell gene *ETV5* did not produce a significant effect.

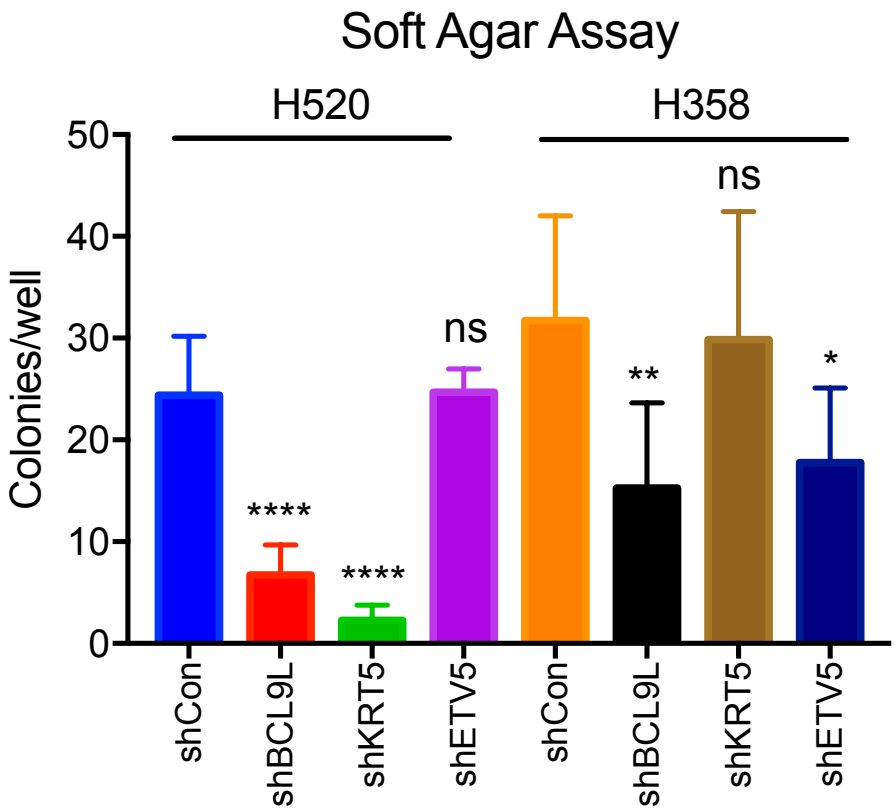

Figure 35. Tumor type specific effects of basal cell or AT2 cell gene knockdown. Soft agar assay in LUSC cell line H520 and LUAD cell line H358 were transfected with shControl, shBCL9L, shKRT5, and shETV5. While both cell lines show colony formation inhibition on knockdown of common gene BCL9L, there is a selective effect for the basal cell gene (Krt5) and AT2 cell gene (ETV5). In the LUSC cell line H520, knockdown of basal cell gene Krt5 produces a decrease in colony formation but there is no significant effect of shETV5. Conversely in LUAD cell line H358, knockdown of AT2 gene ETV5 decreases colony formation while knockdown of basal cell gene Krt5 shows no significant difference from control.

Similarly, knocking down common gene *BCL9L* and AT2 gene *ETV5* significantly reduced colony formation in LUAD cell line H358, whereas knock down of basal cell gene *KRT5* did not produce a significant effect. H520 and H358 shBCL9L cell lines also formed significantly smaller flank tumors in xenograft mice compared to shControl cell lines (Figure 36).

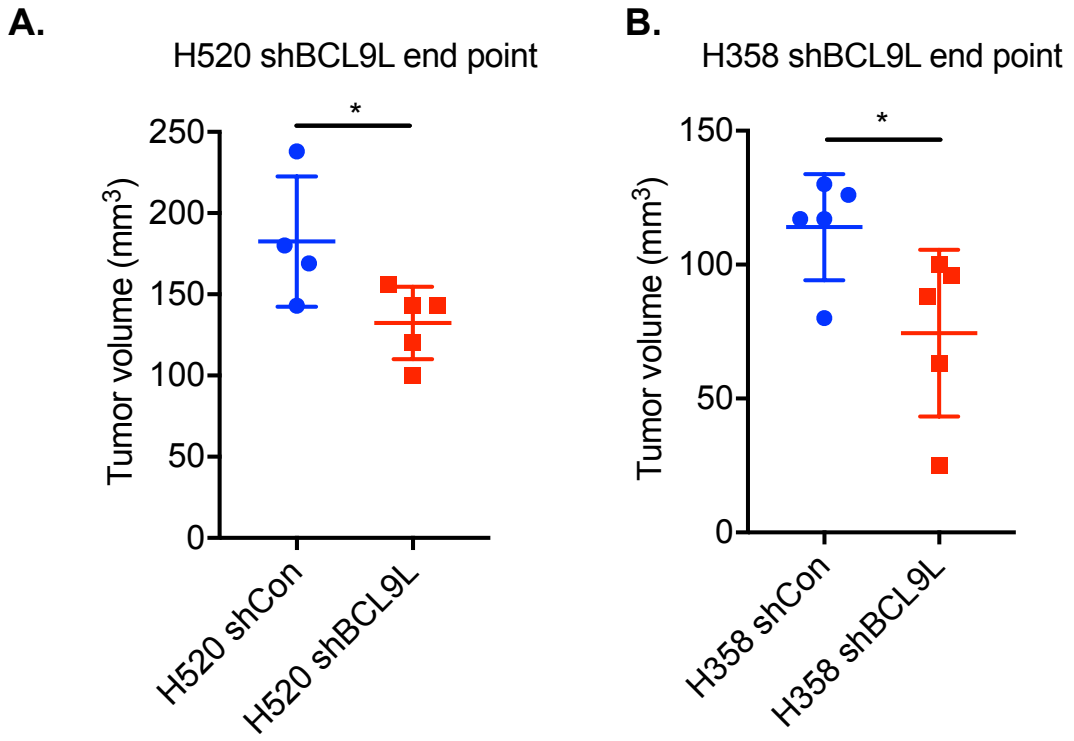

Figure 36. BCL9L knockdown in human lung cancer cell lines.

Comparison of tumor volume of xenografted LUSC cell line (A) H520 shControl and shBCL9L (n=5) and H358 LUAD cell line (B) shControl and shBCL9L (n=5).

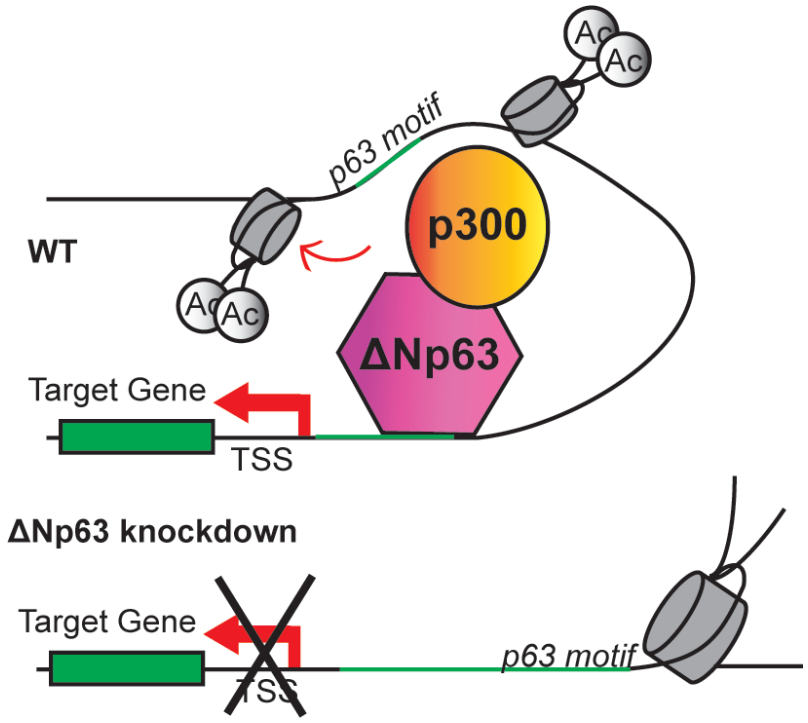

Figure 37. A hypothetical model.

A hypothetical model showing how loss of ΔNp63 leads to a decrease of histone acetylation and gene expression at ΔNp63-regulated genes.

7. Chapter 7: Discussion, Conclusions and Future Directions

Chapter 7: Discussion, Conclusions and Future Directions

The molecular understanding of lung cancer initiation and progression is complex. As new molecular targets are identified for treatment, there remains the exciting possibility to use identified targets for therapeutics and diagnostics. The findings of my thesis would provide new insights into the mechanisms underlying the biology of lung cancer, through determining a novel function of the transcription factor ΔNp63 to regulate cell identity genes in lung stem cells that also have roles in tumor maintenance.

We have shown that ΔNp63 acts in a pro-tumorigenic role in both lung squamous cell carcinoma and lung adenocarcinoma. ΔNp63's role in lung squamous carcinoma has been well documented as a diagnostic marker. Indeed, ΔNp63 has been shown to have high sensitivity and specificity for distinguishing lung squamous cell carcinoma from lung adenocarcinoma, though there are subsets of lung adenocarcinomas that stain positive for ΔNp63. In human squamous cell carcinoma cell lines, we showed that knockdown of ΔNp63 significantly inhibited in vivo tumor growth, through inhibition of cell proliferation and activation of apoptotic processes. We also demonstrate a previously unidentified role of ΔNp63 in lung adenocarcinoma initiation and progression.

Our findings also address the role of p63 isoforms in regulation of lung stem cells. We found that ΔNp63 is the primary isoform that regulates the maintenance and differentiation of tracheal basal stem cells, and to a lesser extent AT2 cells, in the mouse, through regulation of cell identity genes. We suggest that ΔNp63 is a critical regulator for lung stem cell self-renewal and differentiation, controlling important growth and signaling pathways that may also be essential for basal cells and AT2 cells to

transform into cancerous precursors of lung squamous cell carcinoma and adenocarcinoma, respectively.

ΔNp63's role in the distal lung has been implicated by several groups, though their studies have primarily focused on transiently amplified distal lung stem cells that are positive for p63 that arise after lung injury. Our data here suggests a novel mechanism for ΔNp63's role in AT2 cells as we have isolated the specific cell type of AT2 to perform our genetic deletion of ΔNp63. Our mouse model of ΔNp63-LOX-Kras is also a unique approach to identify a tumor initiating role of ΔNp63, presumably through its role in regulation of stem cell signaling pathways that are often co-opted in cancer, such as BCL9L. This suggests that ΔNp63 plays a critical role in the initiation and beginning stages of cancers that are derived from stem cells that require ΔNp63, such as skin, breast, bladder etc.

Our discovery of the role of ΔNp63 in regulation of super-enhancer associated genes shows that ΔNp63 acts as a key transcription factor at enhancer sites to increase gene expression. We have shown this both through ChIP in human cancer cell lines and in an alternative exogenous system utilizing dCas9 technology. As super-enhancer associated genes are increasingly identified as key drivers of individual tumor biology, the targeting of these genes may be key to effective treatment strategies. Increased knowledge about the cell signaling pathways that are essential for cancer initiation and progression are important for the development of new diagnostic and therapeutic modalities.

Previous work in our lab has demonstrated the therapeutic feasibility of targeting ΔNp63 in cancer cells. Venkatanarayan et al demonstrated that deletion of ΔNp63 in the

context of thymic lymphoma can upregulate IAPP metabolic pathways to induce apoptosis of the cell (Venkatanarayan et al., 2015). Interestingly, IAPP has an FDA-approved synthetic analog, Pramlintide, which functioned to induce tumor cell apoptosis in a similar way as deletion of ΔNp63. Napoli et al identified a novel mechanism to target ΔNp63 protein stability by HDAC inhibitors (Napoli et al., 2016). My work contributes further to support the therapeutic strategy of targeting ΔNp63, due to its role in regulation of genes that are key to the function of the cell of origin and are maintained in the development of the cancer.

The work described here can be extended to future studies, as described in the subsequent text. In understanding ΔNp63's role in stem cell biology, we identified an extensive list of genes that are regulated by ΔNp63 in both basal cells and distal lung stem cells. These genes can be further queried to more deeply understand how ΔNp63 maintains the stem cell function. As we have shown that ΔNp63 loss inhibited lung adenoma formation in the mutant Kras mouse model, we are also interested whether this is true in a mouse model of lung squamous cell carcinoma. Mouse models for lung squamous cell carcinoma have not been able to recapitulate the human disease. One approach to understanding if ΔNp63 is required for initiation of lung squamous cell carcinoma would be to cross the $\Delta Np63^{fl/fl}$ mouse to existing lung squamous cell carcinoma mouse models. Likewise, the reverse experiment could be performed which is to over-express ΔNp63 in the lung to observe for increased tumor formation.

Further work can explore if the effectiveness of therapeutically inhibiting ΔNp63 in lung cancer. From previous work in the lab, Pramlintide or HDAC inhibitors could be used to treat human lung cancer cell lines or mouse models of lung cancer. As a major issue of lung cancer mortality is due to a lack of sensitive detection methods,

understanding the early molecular changes that lead to lung cancer could be a strategy to screen for pre-neoplastic lesions in patients, enabling for the determination of patients that require enhanced screening or early treatment.

We propose that ΔNp63 is a master transcription factor in regulation of lung stem cell populations as it regulates genome accessibility of cell-identity genes that are important for promotion of lung cancer initiation and progression. We hope that this discovery provides important new insights about the role of ΔNp63 in the lung and mechanistic insight into how inhibition of ΔNp63 works to inhibit tumorigenesis.

Appendix 1. Oligonucleotide table

Primer Name	Sequence	Function
GAPDH-F	TCA CCA CCA TGG AGA AGG C	Mouse qRT-PCR for GAPDH
GAPDH-R	GCT AAG CAG TTG GTG GTG CA	Mouse qRT-PCR for GAPDH
mETV5-F	TCA GTC TGA TAA CTT GGT GCT TC	Mouse qRT-PCR for ETV5
mETV5-R	GGC TTC CTA TCG TAG GCA CAA	Mouse qRT-PCR for ETV5
mBCL9L-F	AGC AGC ACC TAA TGG GCA AAG	Mouse qRT-PCR for BCL9L
mBCL9L-R	GGA TAA GTC GAA CTC AGG AAT GC	Mouse qRT-PCR for BCL9L
DNp63F1	CAA AAC CCT GGA AGC AGA AA	Mouse qRT-PCR for ΔNp63
TA&DNp63R1	GAG GAG CCG TTC TGA ATC TG	Mouse qRT-PCR for ΔNp63
mTead4-F	TGG ACA TCC GCC AAA TCT ATG	Mouse qRT-PCR for Tead4
mTead4-R	CCC AGA ACT TCA CAA GGA AGA A	Mouse qRT-PCR for Tead4
mDSP-F	GCT GAA GAA CAC TCT AGC CCA	Mouse qRT-PCR for DSP
mDSP-R	ACT GCT GTT TCC TCT GAG ACA	Mouse qRT-PCR for DSP
mPPP1R13L-F	GCC TAC GAG AAA AAG TCT TCA CA	Mouse qRT-PCR for
mPPP1R13L-R	CTC TCT CCA GGG TAA GAG CTG	Mouse qRT-PCR for
mKrt5-F	TCT GCC ATC ACC CCA TCT GT	Mouse qRT-PCR for Krt5
mKrt5-R	CCT CCG CCA GAA CTG TAG GA	Mouse qRT-PCR for Krt5
mSFN-F	GTG TGT GCG ACA CCG TAC T	Mouse qRT-PCR for SFN
mSFN-R	CTC GGC TAG GTA GCG GTA G	Mouse qRT-PCR for SFN
mJAG2-F	TCC TCC TGC TGC TTT GTG AT	Mouse qRT-PCR for JAG2
mJAG2-R	TGT CAG GCA GGT CCC TTG	Mouse qRT-PCR for JAG2
hGAPDH qRT FW	TCT CTG CTC CTC CTG TTC	Human qRT-PCR for GAPDH
hGAPDH qRT Rev	GCC CAA TAC GAC CAA ATC C	Human qRT-PCR for GAPDH
hDNp63-F	GAA AAC AAT GCC CAG ACT CAA	Human qRT-PCR for ΔNp63
hDNp63-R	TGC GCG TGG TCT GTG TTA	Human qRT-PCR for ΔNp63
hCSTA-F	AAA CCC GCC ACT CCA GAA ATC	Human qRT-PCR for CSTA
hCSTA-R	CAC CTG CTC CTA CCT TAA TGT AG	Human qRT-PCR for CSTA
hDSP-F	GCA GGA TGT ACT ATT CTC GGC	Human qRT-PCR for DSP
hDSP-R	CCT GGA TGG TGT TCT GGT TCT	Human qRT-PCR for DSP
hRHOV-F	CCT CAT CGT CAG CTA CAC CTG	Human qRT-PCR for RHOV
hRHOV-R	GAA CGA AGT CGG TCA AAA TCC	Human qRT-PCR for RHOV
hKrt13-F	GAC CGC CAC CAT TGA AAA CAA	Human qRT-PCR for Krt13
hKrt13-R	TCC AGG TCA GTC TTA GAC AGA G	Human qRT-PCR for Krt13
hKrt5-F	CCA AGG TTG ATG CAC TGA TGG	Human qRT-PCR for Krt5
hKrt5-R	TGT CAG AGA CAT GCG TCT GC	Human qRT-PCR for Krt5
hFAM83F-F	CGT CGG CTT CTA CAT GCC C	Human qRT-PCR for
hFAM83F-R	GCT CTA CGT TCT GTC CTG TCA	Human qRT-PCR for
hBCL9L-F	TCT CGC CTA GCA ACT CAA GTC	Human qRT-PCR for BCL9L
hBCL9L-R	GAG CAC CAT TCG TCC CCA C	Human qRT-PCR for BCL9L
hETV5-F	TCA GCA AGT CCC TTT TAT GGT C	Human qRT-PCR for ETV5
hETV5-R	GCT CTT CAG AAT CGT GAG CCA	Human qRT-PCR for ETV5
hTEAD4-F	GAA CGG GGA CCC TCC AAT G	Human qRT-PCR for TEAD4
hTEAD4-R	GCG AGC ATA CTC TGT CTC AAC	Human qRT-PCR for TEAD4
mouse - control gene desert primers	active motif #103720	Mouse ChIP primers – gene desert

mouse + control GAPDH primers	active motif #103726	Mouse ChIP primers +control GAPDH
BCL9L-A FWD set 1	TGG AGG GTT CAT GCT CCT	Mouse ChIP primers BCL9L
BCL9L-A REV set 1	GAT CTC GTT CGC CCT GTT	Mouse ChIP primers BCL9L
BCL9L-B FWD set 1	GAG AGG TAG GAT GGG AGA GAA A	Mouse ChIP primers BCL9L
BCL9L-B REV set 1	GCT GTA GCC CGT GAT GTT	Mouse ChIP primers BCL9L
BCL9L-C FWD set 1	CTG CAG CTG GGC TCT TC	Mouse ChIP primers BCL9L
BCL9L-C REV set 1	GGA GGC TCC TGC ATT CTT G	Mouse ChIP primers BCL9L
BCL9L-D FWD set 3	CCA CTA CGC CTG GCT AAT TT	Mouse ChIP primers BCL9L
BCL9L-D REV set 3	GCA GAT CAC AAG GTC AAG AGT	Mouse ChIP primers BCL9L
KRT5-A FWD set 2	CCT GCA AGT CTG AGG AAT GT	Mouse ChIP primers KRT5
KRT5-A REV set 2	TGT TGA TTT CCA GCC CAT AGT	Mouse ChIP primers KRT5
KRT5-B FWD set 4	CTC GGC TCT CAG CCT CT	Mouse ChIP primers KRT5
KRT5-B REV set 4	GGC ATG GCG ATG ACC TC	Mouse ChIP primers KRT5
KRT5-C FWD set 1	GAG GTG CTG GAG AGA ACA G	Mouse ChIP primers KRT5
KRT5-C REV set 1	CCC AGT TCT GGA AGG GAT AAA	Mouse ChIP primers KRT5
KRT5-D FWD set 1	GAG GAT GTG CAG AGG GAA TG	Mouse ChIP primers KRT5
KRT5-D REV set 1	ACA AAG TGA GTA CCA GGG AAA G	Mouse ChIP primers KRT5
ETV5-A FWD set 3	CGA CCA GAA TTG GGT CTC TT	Mouse ChIP primers ETV5
ETV5-A REV set 3	CAG CGA GTT TGT GTG GAA TG	Mouse ChIP primers ETV5
ETV5-B FWD set 4	AGT CAC CAG TAC GTT CCT TTG	Mouse ChIP primers ETV5
ETV5-B REV set 4	CAG CTA GGC CAA CTG AAA TAG A	Mouse ChIP primers ETV5
ETV5-C FWD set 1	CTC TCG ACT TTC CAC CTC TTT G	Mouse ChIP primers ETV5
ETV5-C REV set 1	GAG GGT AGT TAG GGA ACT CTG T	Mouse ChIP primers ETV5
ETV5-D FWD set 1	TCC CAA AGT GCT GGG ATT AC	Mouse ChIP primers ETV5
ETV5-D REV set 1	GTA GAG ACA GGG TTT CGC TAT G	Mouse ChIP primers ETV5
F1	AAA CTC GAG TGT ACA AAA AAG CAG GCT TTA AAG	dCas9 vector cloning primers
R2	AAA GCT AGC TAA TGC CAA CTT TGT ACA AGA AAG CTG	dCas9 vector cloning primers
F2 ETV5 1	GTA GAT ACA GCA GTA GGA CTT GTT TTA GAG CTA GAA ATA GCA A	dCas9 vector cloning primers
F2 ETV5 2	GTC TGT GTT GTA CTA AAA CTA GTT TTA GAG CTA GAA ATA GCA A	dCas9 vector cloning primers
F2 ETV5 3	GTG TCG TCA AAG TAT AAT CGG TTT TAG AGC TAG AAA TAG CAA	dCas9 vector cloning primers
F2 ETV5 4	GCA GGG ACT TCA AGA GGG CTT GTT TTA GAG CTA GAA ATA GCA A	dCas9 vector cloning primers
R1 ETV5 1	AAG TCC TAC TGC TGT ATC TAC GGT GTT TCG TCC TTT CC	dCas9 vector cloning primers
R1 ETV5 2	TAG TTT TAG TAC AAC ACA GAC GGT GTT TCG TCC TTT CC	dCas9 vector cloning primers
R1 ETV5 3	CGA TTA TAC TTT GAC GAC ACG GTG TTT CGT CCT TTC C	dCas9 vector cloning primers
R1 ETV5 4	AAG CCC TCT TGA AGT CCC TGC GGT GTT TCG TCC TTT CC	dCas9 vector cloning primers
F2 BCL9L 1	GCC TGG AAG TCC CCA CAT CGG TTT TAG AGC TAG AAA TAG CAA	dCas9 vector cloning primers
F2 BCL9L 2	GAG CTC AAA ACC ACC CCA AAG GTT TTA GAG CTA GAA ATA GCA A	dCas9 vector cloning primers

F2 BCL9L 3	GGC TTT CAC GTC ATC ACA GGG TTT TAG AGC TAG AAA TAG CAA	dCas9 vector cloning primers
F2 BCL9L 4	GGG AAG TGT GGA GAG CTA CTG TTT TAG AGC TAG AAA TAG CAA	dCas9 vector cloning primers
R1 BCL9L 1	CGA TGT GGG GAC TTC CAG GCG GTG TTT CGT CCT TTC C	dCas9 vector cloning primers
R1 BCL9L 2	CTT TGG GGT GGT TTT GAG CTC GGT GTT TCG TCC TTT CC	dCas9 vector cloning primers
R1 BCL9L 3	CCT GTG ATG ACG TGA AAG CCG GTG TTT CGT CCT TTC C	dCas9 vector cloning primers
R1 BCL9L 4	AGT AGC TCT CCA CAC TTC CCG GTG TTT CGT CCT TTC C	dCas9 vector cloning primers
F2 Krt5v2 1	GCC AGC CAA AGC ATT TAC CCA GTT TTA GAG CTA GAA ATA GCA A	dCas9 vector cloning primers
F2 Krt5v2 2	GAC CCC TTA ATC CAT GGT CAG GTT TTA GAG CTA GAA ATA GCA A	dCas9 vector cloning primers
F2 Krt5v2 3	GAG GTG GAT GAA TCA TAA CAC GTT TTA GAG CTA GAA ATA GCA A	dCas9 vector cloning primers
F2 Krt5v2 4	GCA AAC ATG AAG GAT GCT CAA GTT TTA GAG CTA GAA ATA GCA A	dCas9 vector cloning primers
R1 Krt5v2 1	TGG GTA AAT GCT TTG GCT GGC GGT GTT TCG TCC TTT CC	dCas9 vector cloning primers
R1 Krt5v2 2	CTG ACC ATG GAT TAA GGG GTC GGT GTT TCG TCC TTT CC	dCas9 vector cloning primers
R1 Krt5v2 3	GTG TTA TGA TTC ATC CAC CTC GGT GTT TCG TCC TTT CC	dCas9 vector cloning primers
R1 Krt5v2 4	TTG AGC ATC CTT CAT GTT TGC GGT GTT TCG TCC TTT CC	dCas9 vector cloning primers
AscIDNp63F	GGG CGC GCC ATG TTG TAC CTG GAA AAC AAT GCC C	dCas9 vector cloning primers
PacIDNp63-R	GTT AAT TAA CTA CTC CCC CTC CTC TTT GAT GCG CTG T	dCas9 vector cloning primers

Bibliography

ABBAS, H. A., BUI, N. H. B., RAJAPAKSHE, K., WONG, J., GUNARATNE, P., TSAI, K. Y., COARFA, C. & FLORES, E. R. 2018. Distinct TP63 Isoform-Driven Transcriptional Signatures Predict Tumor Progression and Clinical Outcomes. *Cancer Res,* 78**,** 451-462.

BIRONZO, P. & DI MAIO, M. 2018. A review of guidelines for lung cancer. *J Thorac Dis,* 10**,** S1556-S1563.

CANCER GENOME ATLAS RESEARCH, N. 2012. Comprehensive genomic characterization of squamous cell lung cancers. *Nature,* 489**,** 519-25.

CATALDO, V. D., GIBBONS, D. L., PEREZ-SOLER, R. & QUINTAS-CARDAMA, A. 2011. Treatment of non-small-cell lung cancer with erlotinib or gefitinib. *N Engl J Med,* 364**,** 947-55.

CHAKRAVARTI, D., SU, X., CHO, M. S., BUI, N. H., COARFA, C., VENKATANARAYAN, A., BENHAM, A. L., FLORES GONZALEZ, R. E., ALANA, J., XIAO, W., LEUNG, M. L., VIN, H., CHAN, I. L., AQUINO, A., MULLER, N., WANG, H., COONEY, A. J., PARKER-THORNBURG, J., TSAI, K. Y., GUNARATNE, P. H. & FLORES, E. R. 2014. Induced multipotency in adult keratinocytes through down-regulation of DeltaNp63 or DGCR8. *Proc Natl Acad Sci U S A,* 111**,** E572-81.

CONDE, E., ANGULO, B., REDONDO, P., TOLDOS, O., GARCIA-GARCIA, E., SUAREZ-GAUTHIER, A., RUBIO-VIQUEIRA, B., MARRON, C., GARCIA-LUJAN, R., SANCHEZ-CESPEDES, M., LOPEZ-ENCUENTRA, A., PAZ-ARES, L. & LOPEZ-RIOS, F. 2010. The use of P63 immunohistochemistry for the identification of squamous cell carcinoma of the lung. *PLoS One,* 5**,** e12209.

DANIELY, Y., LIAO, G., DIXON, D., LINNOILA, R. I., LORI, A., RANDELL, S. H., OREN, M. & JETTEN, A. M. 2004. Critical role of p63 in the development of a normal esophageal and tracheobronchial epithelium. *Am J Physiol Cell Physiol,* 287**,** C171-81.

DRISCOLL, B., KIKUCHI, A., LAU, A. N., LEE, J., REDDY, R., JESUDASON, E., KIM, C. F. & WARBURTON, D. 2012. Isolation and characterization of distal lung progenitor cells. *Methods Mol Biol,* 879**,** 109-22.

DUPAGE, M., DOOLEY, A. L. & JACKS, T. 2009. Conditional mouse lung cancer models using adenoviral or lentiviral delivery of Cre recombinase. *Nat Protoc,* 4**,** 1064-72.

ERAMO, A., HAAS, T. L. & DE MARIA, R. 2010. Lung cancer stem cells: tools and targets to fight lung cancer. *Oncogene,* 29**,** 4625-35.

HANNA, J. M. & ONAITIS, M. W. 2013. Cell of origin of lung cancer. *J Carcinog,* 12**,** 6.

HERBST, R. S., HEYMACH, J. V. & LIPPMAN, S. M. 2008. Lung cancer. *N Engl J Med,* 359**,** 1367-80.

HILTON, I. B., D'IPPOLITO, A. M., VOCKLEY, C. M., THAKORE, P. I., CRAWFORD, G. E., REDDY, T. E. & GERSBACH, C. A. 2015. Epigenome editing by a CRISPR-Cas9-based acetyltransferase activates genes from promoters and enhancers. *Nat Biotechnol,* 33**,** 510-7.

HOWLADER N, N. A., KRAPCHO M, NEYMAN N, AMINOU R, WALDRON W, ALTEKRUSE SF, KOSARY CL, RUHL J, TATALOVICH Z, CHO H, MARIOTTO A, EISNER MP, LEWIS DR, CHEN HS, FEUER EJ, CRONIN KA, EDWARDS BK (EDS). 2011. SEER Cancer Statistics Review, 1975-2008. National Cancer Institute.

JACKSON, E. L., WILLIS, N., MERCER, K., BRONSON, R. T., CROWLEY, D., MONTOYA, R., JACKS, T. & TUVESON, D. A. 2001. Analysis of lung tumor initiation and progression using conditional expression of oncogenic K-ras. *Genes Dev,* 15**,** 3243-8.

JEMAL, A., BRAY, F., CENTER, M. M., FERLAY, J., WARD, E. & FORMAN, D. 2011. Global cancer statistics. *CA Cancer J Clin,* 61**,** 69-90.

JEONG, Y., HOANG, N. T., LOVEJOY, A., STEHR, H., NEWMAN, A. M., GENTLES, A. J., KONG, W., TRUONG, D., MARTIN, S., CHAUDHURI, A., HEISER, D., ZHOU, L., SAY, C., CARTER, J. N., HINIKER, S. M., LOO, B. W., JR., WEST, R. B., BEACHY, P., ALIZADEH, A. A. & DIEHN, M. 2017. Role of KEAP1/NRF2 and TP53 Mutations in Lung Squamous Cell Carcinoma Development and Radiation Resistance. *Cancer Discov,* 7**,** 86-101.

KIM, C. F., JACKSON, E. L., WOOLFENDEN, A. E., LAWRENCE, S., BABAR, I., VOGEL, S., CROWLEY, D., BRONSON, R. T. & JACKS, T. 2005. Identification of bronchioalveolar stem cells in normal lung and lung cancer. *Cell,* 121**,** 823-35.

LOVEN, J., HOKE, H. A., LIN, C. Y., LAU, A., ORLANDO, D. A., VAKOC, C. R., BRADNER, J. E., LEE, T. I. & YOUNG, R. A. 2013. Selective inhibition of tumor oncogenes by disruption of super-enhancers. *Cell,* 153**,** 320-34.

NAPOLI, M., VENKATANARAYAN, A., RAULJI, P., MEYERS, B. A., NORTON, W., MANGALA, L. S., SOOD, A. K., RODRIGUEZ-AGUAYO, C., LOPEZ-BERESTEIN, G., VIN, H., DUVIC, M., TETZLAFF, M. B., CURRY, J. L., ROOK, A. H., ABBAS, H., COARFA, C., GUNARATNE, P. H., TSAI, K. Y. & FLORES, E. R. E. 2016. ΔNp63/DGCR8-dependent microRNAs mediate therapeutic efficacy of HDAC inhibitors in cancer. *Cancer Cell*.

NONAKA, D. 2012. A study of DeltaNp63 expression in lung non-small cell carcinomas. *Am J Surg Pathol,* 36**,** 895-9.

PAUL, M. K., BISHT, B., DARMAWAN, D. O., CHIOU, R., HA, V. L., WALLACE, W. D., CHON, A. T., HEGAB, A. E., GROGAN, T., ELASHOFF, D. A., ALVA-ORNELAS, J. A. & GOMPERTS, B. N. 2014. Dynamic changes in intracellular ROS levels regulate airway basal stem cell homeostasis through Nrf2-dependent Notch signaling. *Cell Stem Cell,* 15**,** 199-214.

REYA, T., MORRISON, S. J., CLARKE, M. F. & WEISSMAN, I. L. 2001. Stem cells, cancer, and cancer stem cells. *Nature,* 414**,** 105-11.

ROCK, J. R., ONAITIS, M. W., RAWLINS, E. L., LU, Y., CLARK, C. P., XUE, Y., RANDELL, S. H. & HOGAN, B. L. 2009. Basal cells as stem cells of the mouse trachea and human airway epithelium. *Proc Natl Acad Sci U S A,* 106**,** 12771-5.

RYAN, M. C., CLELAND, J., KIM, R., WONG, W. C. & WEINSTEIN, J. N. 2012. SpliceSeq: a resource for analysis and visualization of RNA-Seq data on alternative splicing and its functional impacts. *Bioinformatics,* 28**,** 2385-7.

SIEGEL, R. L., MILLER, K. D. & JEMAL, A. 2019. Cancer statistics, 2019. *CA Cancer J Clin,* 69**,** 7-34.

SU, X., CHAKRAVARTI, D., CHO, M. S., LIU, L., GI, Y. J., LIN, Y. L., LEUNG, M. L., EL-NAGGAR, A., CREIGHTON, C. J., SURAOKAR, M. B., WISTUBA, I. & FLORES, E. R. 2010. TAp63 suppresses metastasis through coordinate regulation of Dicer and miRNAs. *Nature,* 467**,** 986-90.

SU, X., CHAKRAVARTI, D. & FLORES, E. R. 2013. p63 steps into the limelight: crucial roles in the suppression of tumorigenesis and metastasis. *Nat Rev Cancer,* 13**,** 136-43.

SU, X., PARIS, M., GI, Y. J., TSAI, K. Y., CHO, M. S., LIN, Y. L., BIERNASKIE, J. A., SINHA, S., PRIVES, C., PEVNY, L. H., MILLER, F. D. & FLORES, E. R. 2009. TAp63 prevents premature aging by promoting adult stem cell maintenance. *Cell Stem Cell,* 5**,** 64-75.

SUR, I. & TAIPALE, J. 2016. The role of enhancers in cancer. *Nat Rev Cancer,* 16**,** 483-93.

SUTHERLAND, K. D. & BERNS, A. 2010. Cell of origin of lung cancer. *Mol Oncol,* 4**,** 397-403.

TRAN, M. N., CHOI, W., WSZOLEK, M. F., NAVAI, N., LEE, I. L., NITTI, G., WEN, S., FLORES, E. R., SIEFKER-RADTKE, A., CZERNIAK, B., DINNEY, C., BARTON,

M. & MCCONKEY, D. J. 2013. The p63 protein isoform DeltaNp63alpha inhibits epithelial-mesenchymal transition in human bladder cancer cells: role of MIR-205. *J Biol Chem,* 288**,** 3275-88.

VENKATANARAYAN, A., RAULJI, P., NORTON, W., CHAKRAVARTI, D., COARFA, C., SU, X., SANDUR, S. K., RAMIREZ, M. S., LEE, J., KINGSLEY, C. V., SANANIKONE, E. F., RAJAPAKSHE, K., NAFF, K., PARKER-THORNBURG, J., BANKSON, J. A., TSAI, K. Y., GUNARATNE, P. H. & FLORES, E. R. 2015. IAPP-driven metabolic reprogramming induces regression of p53-deficient tumours in vivo. *Nature,* 517**,** 626-30.

VISVADER, J. E. 2011. Cells of origin in cancer. *Nature,* 469**,** 314-22.

WANG, S. P., TANG, Z., CHEN, C. W., SHIMADA, M., KOCHE, R. P., WANG, L. H., NAKADAI, T., CHRAMIEC, A., KRIVTSOV, A. V., ARMSTRONG, S. A. & ROEDER, R. G. 2017. A UTX-MLL4-p300 Transcriptional Regulatory Network Coordinately Shapes Active Enhancer Landscapes for Eliciting Transcription. *Mol Cell,* 67**,** 308-321 e6.

WANG, X., LIU, H., SHEN, Y., LI, W., CHEN, Y. & WANG, H. 2018. Low-dose computed tomography (LDCT) versus other cancer screenings in early diagnosis of lung cancer: A meta-analysis. *Medicine (Baltimore),* 97**,** e11233.

WANSLEEBEN, C., BARKAUSKAS, C. E., ROCK, J. R. & HOGAN, B. L. 2013. Stem cells of the adult lung: their development and role in homeostasis, regeneration, and disease. *Wiley Interdiscip Rev Dev Biol,* 2**,** 131-48.

WHYTE, W. A., ORLANDO, D. A., HNISZ, D., ABRAHAM, B. J., LIN, C. Y., KAGEY, M. H., RAHL, P. B., LEE, T. I. & YOUNG, R. A. 2013. Master transcription factors and mediator establish super-enhancers at key cell identity genes. *Cell,* 153**,** 307-19.

XU, X., ROCK, J. R., LU, Y., FUTTNER, C., SCHWAB, B., GUINNEY, J., HOGAN, B. L. & ONAITIS, M. W. 2012. Evidence for type II cells as cells of origin of K-Ras-induced distal lung adenocarcinoma. *Proc Natl Acad Sci U S A,* 109**,** 4910-5.

YAN, W., WISTUBA, II, EMMERT-BUCK, M. R. & ERICKSON, H. S. 2011. Squamous Cell Carcinoma - Similarities and Differences among Anatomical Sites. *Am J Cancer Res,* 1**,** 275-300.

Vita

Sarah Jiaxi Wu was born to parents, Frank Wu and Xuli Wu. In 2006, Sarah graduated from Westwood High School in Austin, TX and attended Rice University, graduating with a B.S. in Biochemistry and Cell Biology in 2010. She enrolled in the MD/PhD program at the University of Texas at Houston in 2010 and joined the lab of Dr. Elsa Flores in 2013. Sarah will graduate from the MD/PhD program in May 2019 and plans to pursue a residency in pathology.